Government of **Western Australia**
Department of **Mines and Petroleum**

RECORD 2015/5

TEMPORAL CONSTRAINTS ON MAGMATISM, GRANULITE-FACIES METAMORPHISM, AND GOLD MINERALIZATION OF THE HERCULES GNEISS, TROPICANA ZONE, ALBANY–FRASER OROGEN

by
CL Kirkland, CV Spaggiari, RH Smithies, MTD Wingate, MT Sweetapple, R Watkins, S Tessalina, and R Creaser



Geological Survey
of Western Australia

Government of **Western Australia**
Department of **Mines and Petroleum**

Record 2015/5

TEMPORAL CONSTRAINTS ON MAGMATISM, GRANULITE-FACIES METAMORPHISM, AND GOLD MINERALIZATION OF THE HERCULES GNEISS, TROPICANA ZONE, ALBANY–FRASER OROGEN

by
CL Kirkland[1], CV Spaggiari, RH Smithies, MTD Wingate, MT Sweetapple[2], R Watkins[3], S Tessalina[4], and R Creaser[5]

1 Now at Centre for Exploration Targeting – Curtin Node, Department of Applied Geology, Western Australian School of Mines, Faculty of Science and Engineering, GPO Box U1987, Perth WA 6845, Australia
2 CSIRO Mineral Resources Flagship, Australian Resources Research Centre, 26 Dick Perry Avenue, Kensington WA 6151, Australia
3 Beadell Resources Limited, 16 Ord Street, West Perth WA 6005, Australia
4 Department of Applied Geology, Curtin University, Kent Street, Bentley WA 6102, Australia
5 University of Alberta, Department of Earth and Atmospheric Sciences, Edmonton, Alberta T6G 2E3, Canada

Perth 2015

Geological Survey of Western Australia

MINISTER FOR MINES AND PETROLEUM
Hon. Bill Marmion MLA

DIRECTOR GENERAL, DEPARTMENT OF MINES AND PETROLEUM
Richard Sellers

EXECUTIVE DIRECTOR, GEOLOGICAL SURVEY OF WESTERN AUSTRALIA
Rick Rogerson

REFERENCE
The recommended reference for this publication is:
Kirkland, CL, Spaggiari, CV, Smithies, RH, Wingate, MTD, Sweetapple, MT, Watkins, R, Tessalina, S and Creaser, R 2015, Temporal constraints on magmatism, granulite-facies metamorphism, and gold mineralization of the Hercules Gneiss, Tropicana Zone, Albany–Fraser Orogen, Record 2015/5, 33p.

National Library of Australia Card Number and ISBN 978-1-74168-635-7

Grid references in this publication refer to the Geocentric Datum of Australia 1994 (GDA94). Locations mentioned in the text are referenced using Map Grid Australia (MGA) coordinates, Zone 51. All locations are quoted to at least the nearest 100 m.

U–Pb measurements were conducted using the SHRIMP II ion microprobes at the John de Laeter Centre of Isotope Research at Curtin University in Perth, Australia.

John de Laeter Centre

Curtin University

Disclaimer
This product was produced using information from various sources. The Department of Mines and Petroleum (DMP) and the State cannot guarantee the accuracy, currency or completeness of the information. DMP and the State accept no responsibility and disclaim all liability for any loss, damage or costs incurred as a result of any use of or reliance whether wholly or in part upon the information provided in this publication or incorporated into it by reference.

Published 2015 by Geological Survey of Western Australia
This Record is published in digital format (PDF) and is available online at <www.dmp.wa.gov.au/GSWApublications>.

Further details of geological products and maps produced by the Geological Survey of Western Australia are available from:
Information Centre
Department of Mines and Petroleum
100 Plain Street
EAST PERTH WESTERN AUSTRALIA 6004
Telephone: +61 8 9222 3459 Facsimile: +61 8 9222 3444
www.dmp.wa.gov.au/GSWApublications

Contents

Figures

Tables

Temporal constraints on magmatism, granulite-facies metamorphism, and gold mineralization of the Hercules Gneiss, Tropicana Zone, Albany–Fraser Orogen

by

CL Kirkland[1], CV Spaggiari, RH Smithies, MTD Wingate, MT Sweetapple[2], R Watkins[3], S Tessalina[4], and R Creaser[5]

Abstract

Craton margins host significant lithospheric discontinuities that focus fluids and heat and which, under favourable circumstances, may become mineralized corridors. Commonly, high-metamorphic-grade terrains are viewed as less prospective for gold mineralization than lower-grade regions. The high-metamorphic-grade Tropicana Zone, located on the southeastern margin of the Yilgarn Craton within the Albany–Fraser Orogen, contains the significant Tropicana gold deposit. The Archean host rocks to the deposit, and similar rocks in the Hercules and Atlantis prospects to the northeast, are mid-amphibolite to granulite-facies gneissic rocks with evidence of partial melting. The Tropicana Zone includes significant low-Si, LILE-enriched granites classed as sanukitoids. Along with their distinctive compositions, the rarity of these rocks within any Archean craton suggests that their granitoid protoliths represent a single suite, emplaced during a single event. Due to the intense granulite-facies overprinting of these rocks, determination of the magmatic protolith age for these sanukitoids is challenging. Nonetheless, the best age estimate for magmatism is 2692 ± 16 Ma, based on U–Pb analysis of the youngest zircons preserving textural evidence of growth within a viscous silicate melt. This result is older than the ages of most other sanukitoids within the Yilgarn Craton. Furthermore, the granulite-facies metamorphic zircon growth in the zone at 2718–2554 Ma is prolonged compared to elsewhere in the Yilgarn Craton. This may indicate that the Archean component of the Tropicana Zone reflects a deeper crustal level or a different part of the Yilgarn Craton, or both. This is consistent with the interpretation that the Tropicana Zone includes a previously unrecognized piece of Yilgarn Craton crust that has been thrust a considerable distance to the northwest, over the Yamarna Terrane of the Yilgarn Craton. Granitic veins dated at c. 1780 Ma have intruded the Archean granitic gneiss and indicate that the Tropicana Zone was close to its present position at or before c. 1780 Ma, given that similar Paleoproterozoic magmatic events are well known from adjacent units within the Albany–Fraser Orogen. Re–Os dating of pyrite coeval with one generation of gold mineralization in these rocks suggests an age of c. 2100 Ma. This mineralization event is distinct from major Proterozoic tectonothermal events known elsewhere in the Albany–Fraser Orogen. Sanukitoid magmas are well known for gold fertility and were likely the source of gold in the Tropicana Zone, which was subsequently remobilized and concentrated into brittle structures. Gold mineralization occurred after peak metamorphic conditions and is significantly younger than gold mineralization within the adjoining Yilgarn Craton.

KEYWORDS: gold, pyrite, zircon

1 Now at Centre for Exploration Targeting – Curtin Node, Department of Applied Geology, Western Australian School of Mines, Faculty of Science and Engineering, GPO Box U1987, Perth WA 6845, Australia

2 CSIRO Mineral Resources Flagship, Australian Resources Research Centre, 26 Dick Perry Avenue, Kensington WA 6151, Australia

3 Beadell Resources Limited, 16 Ord Street, West Perth WA 6005, Australia

4 Department of Applied Geology, Curtin University, Kent Street, Bentley WA 6102, Australia

5 University of Alberta, Department of Earth and Atmospheric Sciences, Edmonton, Alberta T6G 2E3, Canada

Introduction

Craton margins are some of the most dynamic geological environments on the planet, and are typically affected by numerous geodynamic processes. Understanding the geological history of craton margins is complex because no tectonic setting is unique to them, and any settings are likely to change over time. Craton margins can be sites of lithospheric attenuation, rifting and subsequent reattachment, and may be adjacent to subduction zones that redistribute material, or can simply be passive. In addition, where craton margins are accretionary or collisional, exotic terranes may be transferred to them.

Craton margins are the sites of major lithospheric discontinuities that can direct element mobility, heat flow, material (recycling), and magma (reworking and new mantle input) and, under favourable circumstances, these discontinuites can become mineralization corridors (Hronsky et al., 2012). Craton margins have changed over geological time, reflecting high Archean mantle temperatures with low mantle viscosity compared to relatively low Proterozoic mantle temperatures (Goldfarb et al., 2001). Slower or intermittent Archean subduction, compared to steep Proterozoic subduction, may be expected to result in distinctly different craton margin architectures and processes (Groves et al., 2005).

The reworked margins of Archean cratons are increasingly recognized as key regions where upgrading of ancient mineral endowments to economically viable levels can occur (e.g. Sillitoe, 2008; Gazley et al., 2011). However, other processes along craton margins, such as terrane transfer, may also play important roles in delivering mineral endowment to the edges of cratons (Coney et al., 1980; Solomon, 1990; Tohver et al., 2004).

One such example of a dynamic craton margin is the Albany–Fraser Orogen, adjacent to the southern and southeastern margins of the Archean Yilgarn Craton in Western Australia (Fig. 1; Myers, 1990; Beeson et al., 1995; Spaggiari et al., 2011, 2014a). This Paleoproterozoic to Mesoproterozoic orogen has extensively modified the Yilgarn Craton margin during episodes of juvenile asthenospheric addition and significant reworking of pre-existing Archean rocks (Spaggiari et al., 2011; Kirkland et al., 2011a,b). With the discovery of the estimated 8 million ounce Tropicana gold deposit (Doyle et al., 2013) and the estimated 14.6 Mt combined Nova–Bollinger Ni–Cu–Co deposit in the Fraser Zone (Sirius, 2013), the orogen has recently gained considerable economic importance. Based on structural and geochronological constraints, gold mineralization at Tropicana is generally considered to post-date peak metamorphism and is younger than other gold deposits in the Yilgarn Craton (Doyle et al., 2008, 2009, 2013, 2015). However, the tectonic setting for this mineralization event is unknown. An understanding of the ages and compositions of basement rocks on this margin, along with their relationship to other known parts of the Yilgarn Craton, has important implications for constraining gold exploration models.

The exploration leases within the Neale Project lie about 60 km northeast of the Tropicana gold deposit. This area preserves disseminated and vein-hosted gold mineralization associated with the Hercules Shear Zone, where results of up to 160 g/t gold have been recorded (Watkins, 2012). To improve our understanding of the geological evolution of this region and its relationship to gold mineralization, we studied numerous samples from seven diamond drillcores from two prospects (Hercules and Atlantis) within the Neale Project area in the Tropicana Zone (Figure 1). In this contribution, we report SIMS (SHRIMP) U–Pb zircon geochronology of eight samples from five of the diamond cores, and Re–Os geochronology on two fractions of a pyrite sample from one drillcore. We also report details of whole-rock geochemistry on these diamond cores.

The Tropicana Zone and its regional context

The Tropicana Zone lies in the Great Victoria Desert in the northeastern segment of the Albany–Fraser Orogen (Fig. 1) and is largely covered by sand-dominated regolith, and in part by Permian glacigene sedimentary rocks. Because of this poor exposure, the geological history and architecture of the zone has been based largely on the interpretation of geophysical data, including high-resolution magnetic and gravity data, deep-crustal seismic reflection data, limited outcrops, drillcores, and correlations with other regions within the orogen (Occhipinti et al., 2014; Spaggiari et al., 2011; Spaggiari and Occhipinti, 2014).

The Albany–Fraser Orogen is dominated by Paleoproterozoic to Mesoproterozoic igneous rocks and older Archean crust with variable degrees of reworking. The Kepa Kurl Booya Province (KKBP) reflects the basement component of the orogen, which has been reworked during the Proterozoic, and its association to the Yilgarn Craton is cryptic (Spaggiari et al., 2009, 2014b). The KKBP comprises four fault-bound tectonostratigraphic packages, named the Tropicana, Biranup, Fraser, and Nornalup Zones (Fig. 1) (Spaggiari et al., 2014c). The Biranup Zone is dominated by Paleoproterozoic (1800–1620 Ma) basement rocks generated through recycling of dominantly Archean felsic material in several episodes. The Nornalup Zone is intruded by voluminous granitic rocks of the Mesoproterozoic 1330–1280 Ma Recherche Supersuite and the 1200–1140 Ma Esperance Supersuite granites (Nelson et al., 1995; Spaggiari et al., 2014b; Smithies et al., 2014). The structurally bound, gabbro-dominated 1305–1280 Ma Fraser Zone lies between the Biranup and Nornalup Zones (Figure 1), and is underlain by reworked Yilgarn Craton and Biranup Zone crust (Spaggiari et al., 2014c; Brisbout et al., 2014). In addition to the KKBP is another unit, the Northern Foreland, which contains metamorphic rocks that are readily distinguished as formerly part of the Yilgarn Craton, whereas those of the KKPB are more intensely reworked (Kirkland et al., 2011a,b; Smithies et al., 2014).

The main tectonic and metamorphic features of the Albany–Fraser Orogen result from several Proterozoic

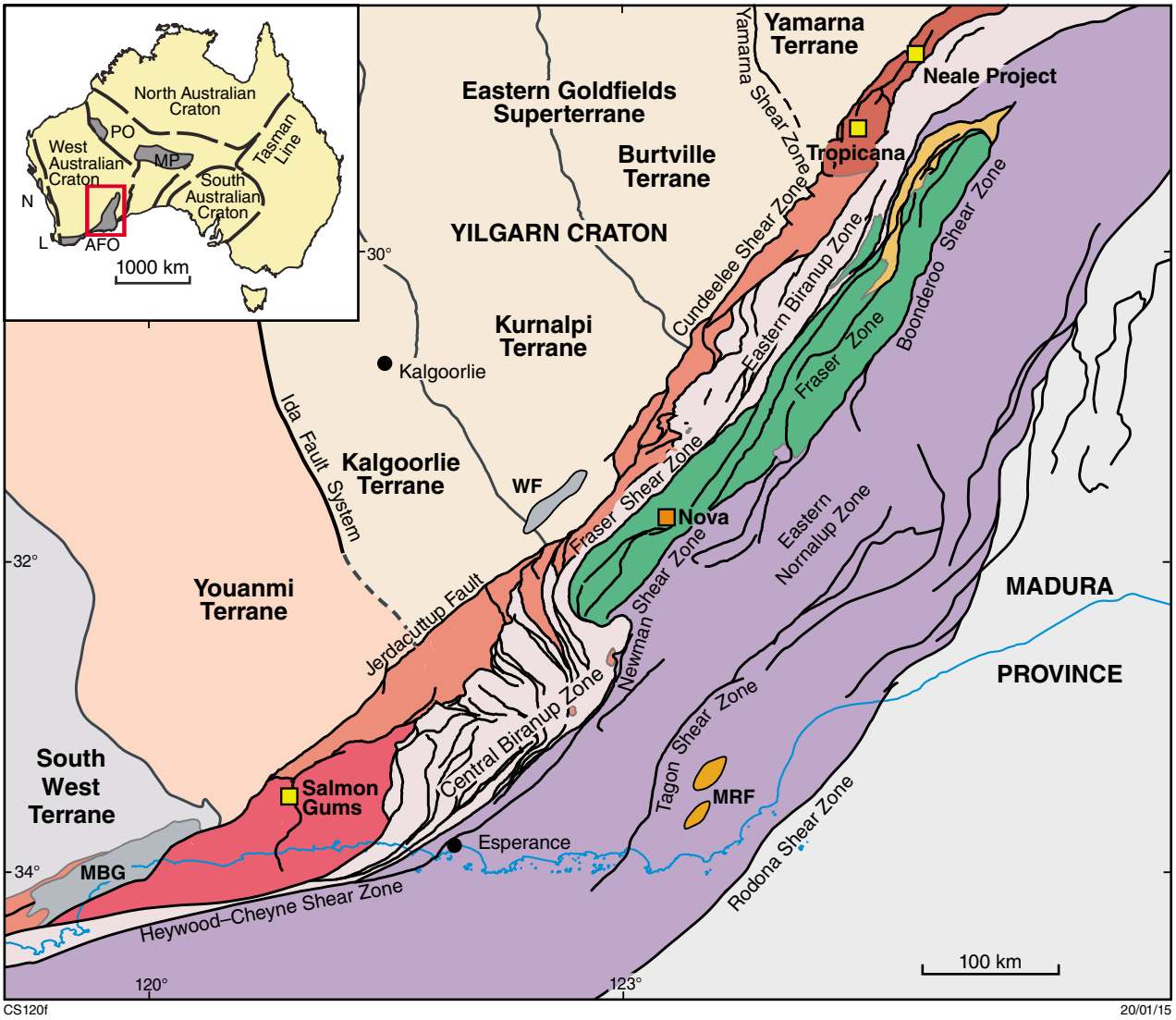

Figure 1. Simplified pre-Mesozoic interpreted bedrock geology of the east Albany–Fraser Orogen (from Spaggiari et al., 2011) and tectonic subdivisions of the Yilgarn Craton (modified from Geological Survey of Western Australia, 2011; Cassidy et al., 2006; Pawley et al., 2012). Abbreviations used: MBG – Mount Barren Group; WF – Woodline Formation; MRF – Mount Ragged Formation; AFO – Albany–Fraser Orogen; MP – Musgrave Province; PO – Paterson Orogen; L – Leeuwin Province; N – Northampton Province

tectonic events. Paleoproterozoic events include mainly granitic magmatism and extensional tectonics at 1815–1800 Ma (the Salmon Gums Event) and 1780–1760 Ma (the Ngadju Event), culminating in the 1710–1650 Ma Biranup Orogeny, which includes the c. 1680 Ma compressional Zanthus Event (Kirkland et al., 2011a; Spaggiari et al., 2014b). Orogen-wide extension during these events formed the c. 1815–1600 Ma Barren Basin (Spaggiari et al., 2014a). Mesoproterozoic tectonic events include formation of the Arid Basin (1600–1305 Ma), and Stages I (1330–1260 Ma) and II (1225–1140 Ma) of the Albany–Fraser Orogeny (Clark et al., 2000; Kirkland et al., 2011a; Spaggiari et al., 2014a,b). Stage I of the Albany–Fraser Orogeny was dominated by coeval felsic and mafic magmatism accompanied by deformation and high-temperature and moderate- to high-pressure metamorphism (Nelson et al., 1995; Clark et al, 1999, 2000; Oorschot, 2011; Clark et al., 2014). Stage II involved intense deformation dominated by thrusting, high-temperature and moderate-pressure metamorphism, and primarily felsic magmatism after c. 1200 Ma (Dawson et al., 2003; Spaggiari et al., 2009, 2011). The complex thermal history of the Albany–Fraser Orogen has caused significant new mineral growth during these events. However, the extent to which this Proterozoic history has been responsible for gold metallogenesis in the northeastern part of the orogen has previously been unclear.

Peak metamorphic conditions for the Tropicana Zone are poorly constrained. However, Doyle et al. (2015) interpreted granulite-facies conditions on the basis of charnockitic gneiss with abundant hypersthene, quartz, and plagioclase, and widespread partial melting. Leucosomes are texturally continuous with the gneissosity or intruded parallel to the axial plane of intrafolial folds indicating syndeformational emplacement during peak metamorphism. Occurrences of two-pyroxene mafic gneiss are also consistent with granulite-facies pressures and temperatures. Garnet–clinopyroxene and garnet–amphibole geothermometers suggest a minimum temperature of around 650°C at 5 kbar (Saunders, 2006) during retrogression under amphibolite-facies conditions.

Lithological units of the Tropicana Zone

The Tropicana Zone comprises amphibolite- to granulite-facies Archean basement rocks of the Tropicana Gneiss and Hercules Gneiss (see Neale Project area, below), locally overlain by greenschist- to amphibolite-facies rocks of the Lindsay Hill Formation (Barren Basin), and intruded by Paleoproterozoic granitic rocks related to the adjacent Biranup Zone (Fig. 2). The c. 2640 Ma Tropicana Gneiss consists of amphibolite- to granulite-facies, locally migmatitic quartzofeldspathic gneiss, garnet-bearing gneiss, mafic to ultramafic gneiss, metachert, and meta-iron formation (including grunerite–quartz±garnet), and was subject to gold mineralization during a low-grade fluid movement event at c. 2500 Ma (Doyle et al., 2009, 2014; Fox-Wallace, 2010; Blenkinsop and Doyle, 2014). The host rocks to the Tropicana deposit yield U–Pb zircon ages between c. 2700 and 2600 Ma, and the timing of peak granulite-facies metamorphism is loosely constrained between c. 2638 and 2520 Ma (Doyle et al., 2014; 2015).

The overlying metasedimentary rocks of the Lindsay Hill Formation (Barren Basin) have a maximum depositional age of 1752 ± 19 Ma (Spaggiari et al., 2014a). Volcanosedimentary and intrusive rocks of the c. 1760 Ma Voodoo Child Formation include dacite, leucogabbro, and mafic–ultramafic rocks, and are interpreted to have formed in a small pull-apart basin (Less, 2013). Paleoproterozoic intrusive rocks in the Tropicana Zone include the c. 1763 Ma McKay Creek Metasyenogranite (Kirkland et al., 2012) and the c. 1708 Ma Bobbie Point Metasyenogranite (Kirkland et al., 2010). Structurally overlying the Tropicana Zone to the east, the Biranup Zone includes metagranodiorite, quartz metadiorite, and metadiorite of the 1815–1800 Ma Black Dragon Gneiss (Blenkinsop and Doyle, 2014), and metagranite and metagabbro dated between c. 1690 and 1670 Ma in the Pleiades Lakes area (Spaggiari et al., 2011; Stokes, 2014; http://www.dmp.wa.gov.au/geochron/). Unlike their amphibolite- to granulite-facies Biranup Zone counterparts to the south, the metamorphic grade of these rocks is greenschist to amphibolite facies.

Architecture of the Tropicana Zone

Recently acquired deep-crustal seismic data have provided great insight into the structural architecture of the Tropicana Zone, particularly when combined with magnetic and gravity data, and information from drillcores and sparse outcrops (Occhipinti et al., 2014). Seismic line 12GA-T1 shows that the Tropicana Zone and northeastern Biranup Zone lie above a distinct structure with an apparent shallow southeast dip, the Plumridge Detachment. Above this detachment the Tropicana Zone thins towards the northwest, from about 10 km depth to about 3.6 km, where the seismic line terminates below the Gunbarrel Basin (Occhipinti et al., 2014). The Plumridge Detachment separates the Tropicana Zone from the underlying reworked Yamarna Terrane of the Eastern Goldfields Superterrane (Occhipinti et al., 2014). This structure is interpreted to have formed at c. 2520 Ma, synchronous with exhumation of the Tropicana Gneiss into greenschist-facies crustal levels, and with gold mineralization at Tropicana (Blenkinsop and Doyle, 2014; Doyle et al., 2014, 2015; Occhipinti et al., 2014).

Major shear zones are generally northeast trending and southeast dipping (Fig. 2). Some shear zones are interpreted to sole into the Plumridge Detachment, and others are clearly younger as they either contain or cut Paleoproterozoic rocks (Occhipinti et al., 2014). The difference in metamorphic grade provides a useful marker in separating older, pre-detachment structures from younger Paleoproterozoic or Mesoproterozoic structures in the Tropicana Zone. These include the Black Dragon, Blue Robin, and Sydney Simpson Shear Zones that separate the Tropicana Zone from the Biranup Zone (Fig. 2).

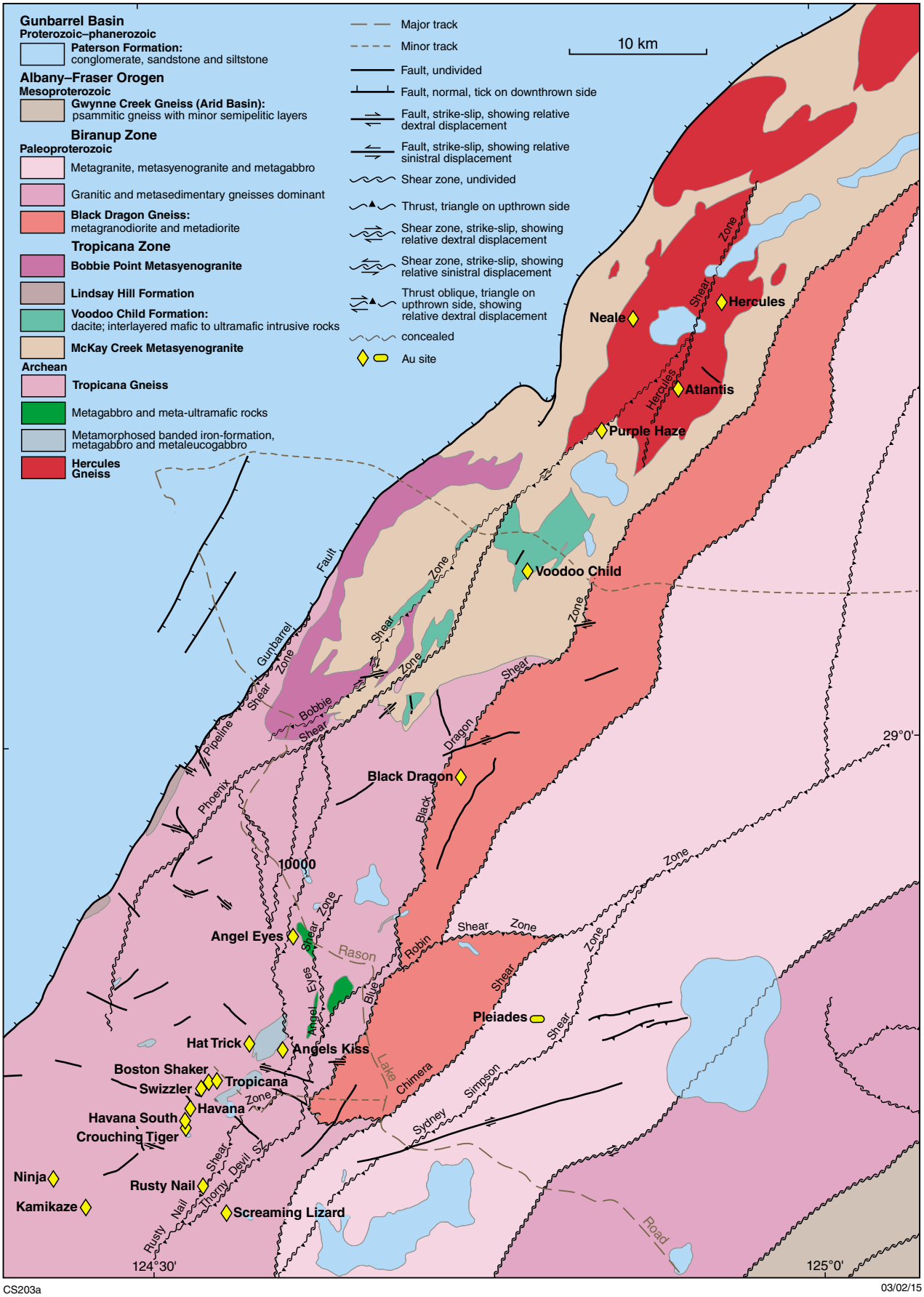

Figure 2. Pre-Mesozoic interpreted bedrock geology of the northeastern Albany–Fraser Orogen including the Tropicana Zone (simplified from Spaggiari and Occhipinti, 2014)

Neale Project area: Hercules Gneiss

The Neale Project area lies about 60 km northeast of the Tropicana gold mine, and includes three prospects: Neale, Hercules, and Atlantis (Fig. 2). The area lies completely beneath thick regolith cover and locally beneath Permian Paterson Formation sedimentary rocks and thick regolith cover. However, basement structures are distinguishable in aeromagnetic data as a northeast-trending zone of moderate magnetic intensity, which includes the Hercules Shear Zone (Fig. 3). In 2011, seven diamond drillcores were obtained from the Hercules and Atlantis prospects, funded in part through the Exploration Incentive Scheme co-funded drilling program (Fig. 2; Goddard, 2010). The analysis of these cores has provided valuable information towards understanding the evolution of the Tropicana Zone and relationships to gold mineralization at Tropicana.

All seven cores contain felsic to intermediate granitic gneiss locally interlayered with mafic (gabbroic) gneiss, here named the Hercules Gneiss. The Hercules Gneiss typically has a well-defined layered gneissic fabric, locally with blue quartz (Fig. 4a), with a variable but dominantly southeast dip (Figs 5 and 6). This gneissic fabric is the oldest recognizable component, and is locally folded (Fig. 4b). It is overprinted by an early phase of alteration (e.g. red-stained feldspars) that is in turn cut by a mylonitic fabric with a dominant subvertical to southeast dip (Figs 4c and 5). Mylonitization is inferred to have facilitated fluid movement and the formation of hydrous biotite and sericite, and possibly disseminated sulfide minerals (Fig. 4d).

The fabrics are cut by sulfide-bearing quartz veins (including Re–Os sample GSWA 192522, Fig. 4e) and calcite veins, and by discrete zones of brecciation. From crosscutting relationships, it appears likely that a period of alternating shearing and alteration was followed by quartz veining and brecciation. The gneissic fabric is also cut by dolerite intrusions that also are cut by quartz and calcite veins, although it is not clear whether these veins pre- or post-date mylonitization. However, unfoliated microgranite veins cut both the gneissosity and the mylonitic fabric, and contain younger quartz veins with sulfides and small discrete shear zones (Figs 4f and 5). To provide context for the geochronology samples, the lithological and structural relationships in individual cores are described below, listed in Table 1, and illustrated in Figures 5 and 6.

Hercules prospect

Drillcore NLD210

NLD210 was drilled to a depth of 190 m and the core consists of medium-grained quartzofeldspathic to dioritic orthogneiss structurally overlying medium-grained dioritic to amphibolitic gneiss (Fig. 5). These two rock types are separated (at 90–93 m) by a steeply east-dipping, muscovite- and sericite-bearing shear zone that cuts the gneissic foliation in both gneisses. The dioritic to amphibolitic gneiss is cut by an approximately 5 m thick dolerite intrusion that in turn is cut by mm- to cm-scale quartz and calcite veins, which also cut the mylonitic fabric in the shear zone. Quartz veins cut other smaller east-dipping shear zones, although some appear to be synchronous with ductile shear zones. Gold mineralization between 164 and 175 m depth is hosted within quartz–sulfide veins. All foliations are cut by alteration in the form of pyrite veinlets, thin epidote veins, quartz veins, and quartz–calcite veins. Pyrite occurs mainly in quartz veins but is also disseminated within the gneisses. Two U–Pb zircon geochronology samples were studied from this drillcore.

Drillcore NLD097

NLD097 was drilled to a depth of 141.90 m (Fig. 5). The core is dominated by a medium- to coarse-grained granitic gneiss of mainly intermediate composition that is similar to the lower lithology in NLD210. The granitic gneiss contains distinctive, abundant blue quartz, localized euhedral garnet, and sulfide minerals. It has a well-developed subhorizontal to gently east-dipping gneissosity that is locally cut by mylonite zones. The gneissosity is also crosscut by monzogranite and microgranite veins that are generally unfoliated and which locally contain small ductile shear zones hosting biotite and pyrite (Fig. 4f). The microgranite veins are themselves crosscut by thin veins of K-feldspar, quartz, and epidote, which also contain sulfide minerals. Two U–Pb zircon geochronology samples were studied from this drillcore.

Atlantis prospect

Drillcore NLD080

Drillcore NLD080 extends to a depth of 96.35 m and is the core dominated by a felsic to intermediate mylonite gneiss (Fig. 6), the protolith of which was probably an igneous rock (Fig. 6). Locally, small fabric-parallel quartzofeldspathic leucosomes with biotite selvedges suggest the gneiss has undergone small degrees of in situ partial melting. The mylonitic foliation is subvertical, and kinematic observations of porphyroclasts and shear bands indicate a dextral sense of movement, with southeast side down. The movement direction is based on the direction of the long axes of the porphyroclasts and the alignment of matrix minerals within the mylonitic foliation. The mylonitic foliation also crosscuts an earlier phase of alteration, visible as red staining on feldspars, and on quartz veins that, based on their morphology, probably represent former tension gashes. Towards the base of drillcore, a red breccia zone crosscuts the mylonitic fabric. Sulfide minerals are disseminated throughout the mylonite. Two U–Pb zircon samples were studied from the drillcore.

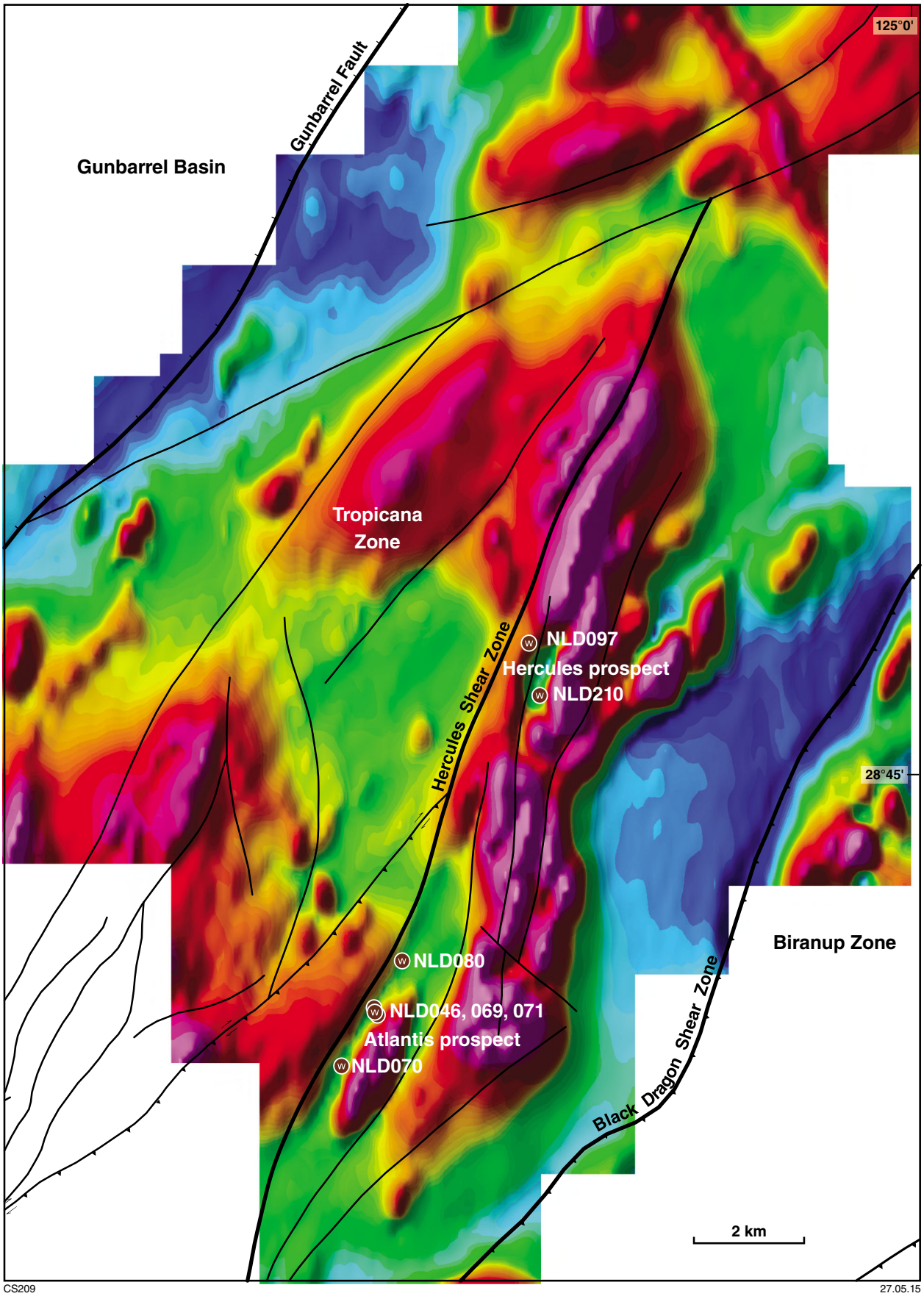

Figure 3. Reduced-to-pole aeromagnetic image of the Neale Project area showing simplified interpreted structures (from Spaggiari and Occhipinti, 2014), Hercules and Atlantis prospects, and locations of drillcores. Aeromagnetic data is the Neale survey 70053, which was flown to infill 400 m government data to 200 m line spacing

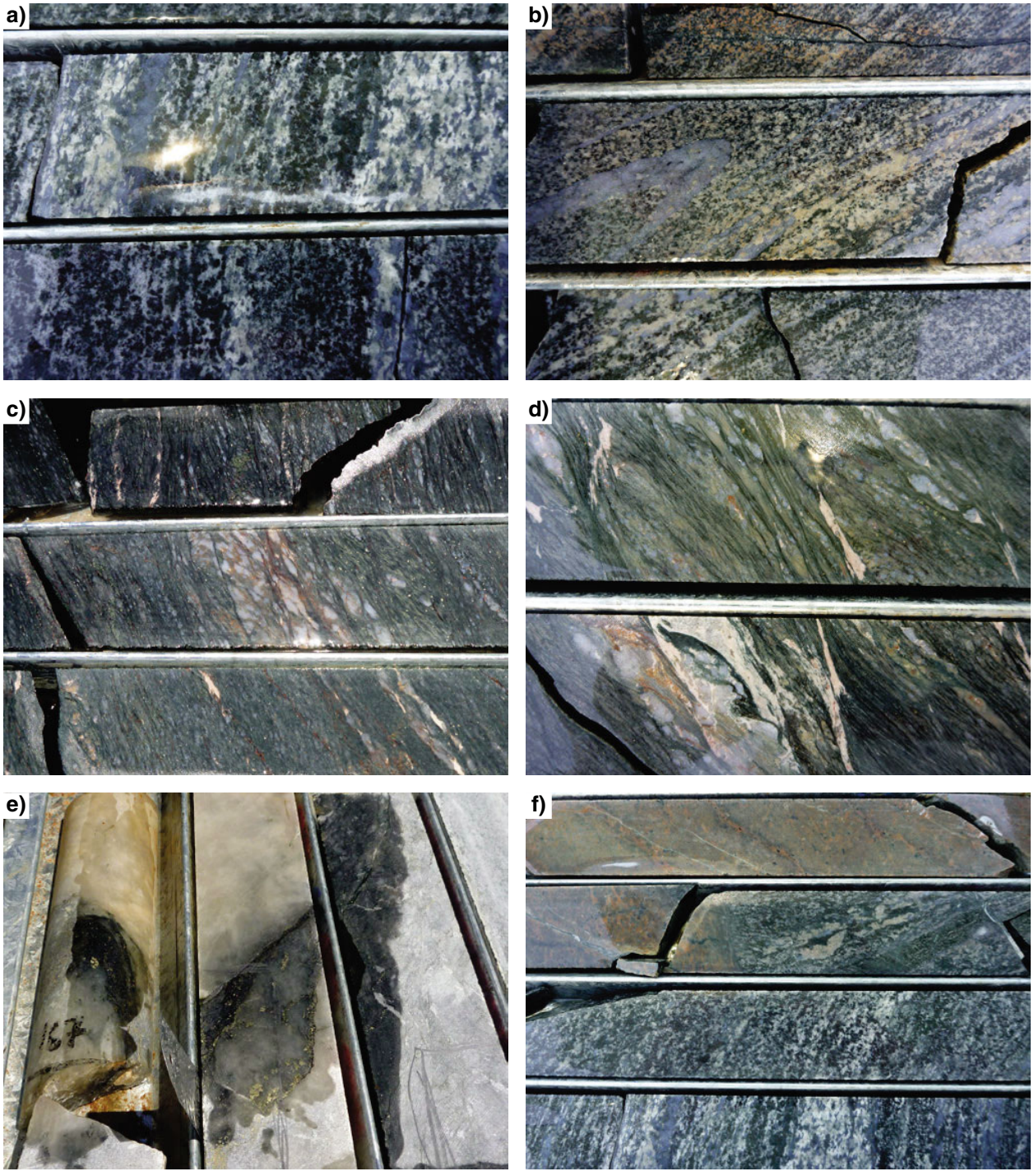

Figure 4. **Photographs of diamond cores: a) Typical gneissic fabric with blue quartz; granitic gneiss in upper section of drillcore NLD097, Hercules Prospect; b) Small-scale, early tight folds in granitic gneiss in drillcore NLD070, Atlantis Prospect. The gneissic foliation is axial planar to these folds; c) Mylonitic fabric overprinting granitic gneiss in drillcore NLD046, Atlantis Prospect; d) Mylonitic fabric with disseminated sulfides in drillcore NLD070, Atlantis Prospect; e) Quartz veins with gold-bearing pyrite from the gold mineralized horizon in the lower part of drillcore NLD210, Hercules Prospect. The core sampled for Re–Os dating (GSWA 192522) is shown in the centre; f) Microgranite vein cutting granitic gneiss in drillcore NLD097, Hercules Prospect**

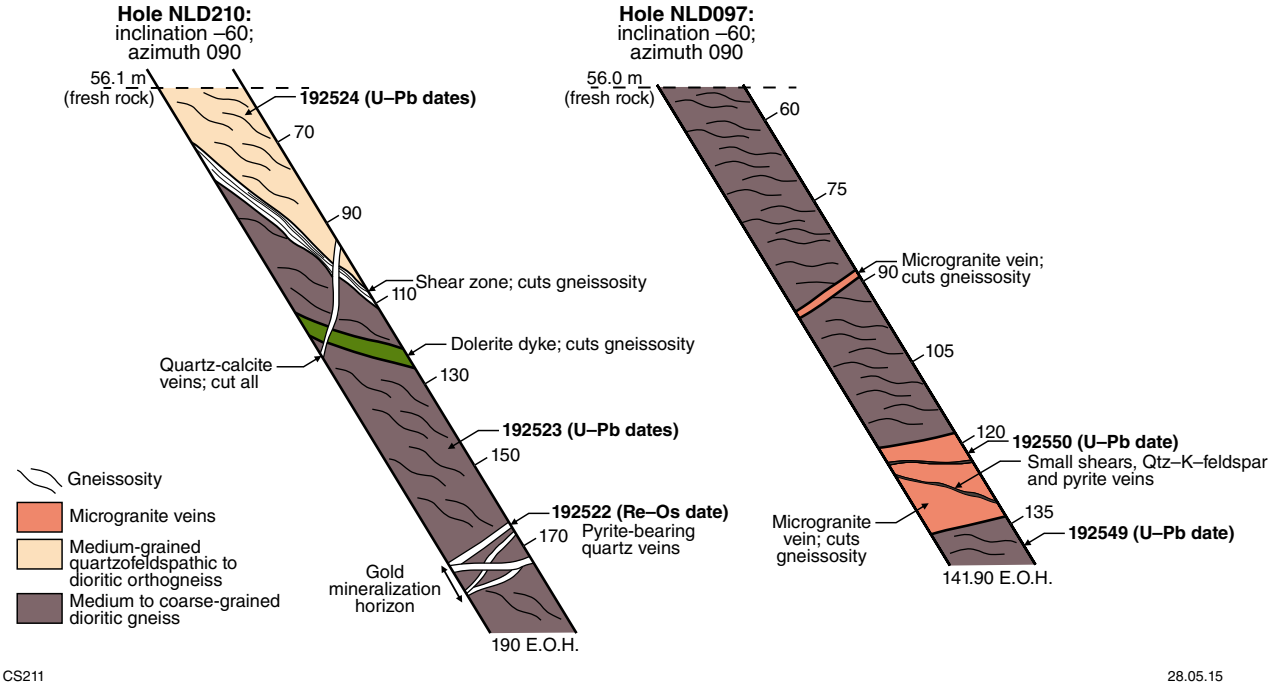

Figure 5. Schematic diagrams of the two diamond drillcores NLD210 (left) and NLD097 (right) from the Hercules Prospect, showing crosscutting relationships and locations of geochronology samples

Drillcore NLD071

Drillcore NLD071 extends to a depth of 122 m (Fig. 6). The upper section of the core is a weathered granitic gneiss, with fresh rock present below about 51 m. The granitic gneiss preserves a gneissosity that generally dips moderately to the southeast. Thin epidote veins are developed both parallel and oblique to the gneissic foliation. Abundant, small, disseminated sulfide grains are present throughout the gneiss. The gneissic fabric is crosscut by steeply northwest-dipping shear zones, quartz veins that are also sulfide-bearing, and locally by pink K-feldspar-bearing veins. Separated by a shear zone, the lowermost 10 m of the core contains fine-grained mafic rock that becomes more coarse grained with depth (Fig. 6). This intrusion is most likely the same intrusion present in the upper section of NLD069 (see below).

Drillcore NLD046

Drillcore NLD046 extends to a depth of 294.65 m (Fig. 6). There is considerable lithological variety within this core. The upper section and structurally highest section within this core consists of a medium-grained gneiss, which has an intermediate composition, is interpreted to have formed from a granitic protolith, and exhibits a strong subvertical foliation that is in part mylonitic. For the most part, the mylonitic fabric is defined by quartz–sericite layers and local feldspar porphyroclasts. Localized S–C structures indicate dextral, southeast-side-down movement, although the mylonitic fabric is also locally folded. The movement direction is inferred from the orientation of the long axes and alignment of the minerals in the mylonite. Sulfides are disseminated throughout the gneiss. At about 180–183 m depth, the gneiss is interlayered with a medium- to fine-grained mafic rock, which also contains disseminated sulfide minerals. At about 200 m depth, the foliation becomes subhorizontal, implying folding. Structurally below this fold hinge, coarser grained granitic gneiss is interlayered with metagabbroic gneiss that contains about 30% coarse, rounded blebs of garnet locally overgrown by chlorite. This rock is interpreted as a mafic granulite that has undergone retrogression and overprinting by a lower-grade retrograde assemblage of chlorite, epidote, and amphibole. It also contains sulfide minerals within thin blue quartz veins that cut the foliation. The interlayered gneiss is also cut by late pink or quartz-rich veins, some of which contain pyrite. Below 283 m, the core consists of medium-grained monzodiorite gneiss. A single sample for U–Pb zircon geochronology was recovered from this core.

Drillcore NLD069

Drillcore NLD069 extends to a depth of 136.25 m (Fig. 6). The structural top of the core contains an unfoliated mafic rock, probably representing an intrusion similar to that in NLD071. The mafic unit is cut by thin quartz, K-feldspar, and epidote–chlorite veins. Structurally below this mafic unit is a medium-grained granitic gneiss with biotite-rich layers, and finer grained mafic layers. The gneissosity in these interlayered units is steeply dipping and is locally cut by thick quartz veins. At about 81 m depth, the gneissosity is cut by an approximately 10 cm-thick quartz vein and an associated steeply dipping mylonitic foliation.

Table 1. Summary of SHRIMP U–Pb geochronology of the Hercules Gneiss

Sample ID	Lithology	Drillcore ID	Location	Drillcore depth (m)	Magmatic protolith component Group I	Granulite-grade zircon Group M (1)			Metamorphism Group M2	GSWA Geochronology record
					Age (Ma) ± 2σ	Max age ± 1σ	Min age ± 1σ	Youngest group	Age (Ma) ± 2σ	
192523	amphibolitic gneiss	NLD210	MGA Zone 51, 688765E 6819500N	143.90 – 144.05	2692 ± 16	2690 ± 12	2608 ± 11	2631 ± 7	1770 ± 46	Wingate, MTD, Kirkland, CL and Spaggiari, CV 2014, 192523: amphibolitic gneiss, Hercules prospect; Geochronology Record 1187: Geological Survey of Western Australia, 5p.
192524	quartzofelds-pathic gneiss	NLD210	MGA Zone 51, 688765E 6819500N	59.95 – 60.20	≥ 2677	2677 ± 117	2603 ± 12	2634 ± 8		Wingate, MTD, Kirkland, CL and Spaggiari, CV 2014, 192524: quartzofeldspathic gneiss, Hercules prospect; Geochronology Record 1188: Geological Survey of Western Australia, 4p.
192530	mylonitic metagranite	NLD080	MGA Zone 51, 686263E 6814695N	60.20 – 60.30	2795 ± 12	2636 ± 8	2566 ± 4	2623 ± 7		Wingate, MTD, Kirkland, CL and Spaggiari, CV 2014, 192530: mylonitic metagranite, Hercules prospect; Geochronology Record 1189: Geological Survey of Western Australia, 4p.
192531	metagranite	NLD080	MGA Zone 51, 686263E 6814695N	68.35 – 68.50	≥ 2683	2683 ± 10	2585 ± 16	2624 ± 13		Kirkland, CL, Wingate, MTD and Spaggiari, CV 2014, 192531: metagranite, Atlantis prospect; Geochronology Record 1181: Geological Survey of Western Australia, 4p.
192532	granitic gneiss	NLD071	MGA Zone 51, 685817E 6813714N	63.80 – 64.10	2826 ± 166	2718 ± 95	2580 ± 13	2611 ± 17		Kirkland, CL, Wingate, MTD and Spaggiari, CV 2013, 192532: granitic gneiss, Atlantis prospect; Geochronology Record 1182: Geological Survey of Western Australia, 4p.
192549	granitic gneiss	NLD097	MGA Zone 51, 688568E 6820449N	139.12 – 139.44	≥ 2644	2644 ± 12	2554 ± 56	2594 ± 18		Kirkland, CL, Wingate, MTD and Spaggiari, CV 2014, 192549: monzodioritic gneiss, Hercules prospect; Geochronology Record 1183: Geological Survey of Western Australia, 4p.
192550	microgranite vein	NLD097	MGA Zone 51, 688568E 6820449N	121.34 – 121.44	1783 ± 3					Kirkland, CL, Wingate, MTD and Spaggiari, CV 2014, 192550: monzogranite vein, Hercules prospect; Geochronology Record 1184: Geological Survey of Western Australia, 4p.
192552	meta-granodiorite	NLD046	MGA Zone 51, 685753E 6813844N	289.60 – 289.90	2726 ± 14	2698 ± 26	2615 ± 25	2641 ± 8		Wingate, MTD, Kirkland, CL and Spaggiari, CV 2014, 192552: monzodioritic gneiss, Atlantis prospect; Geochronology Record 1185: Geological Survey of Western Australia, 4p.

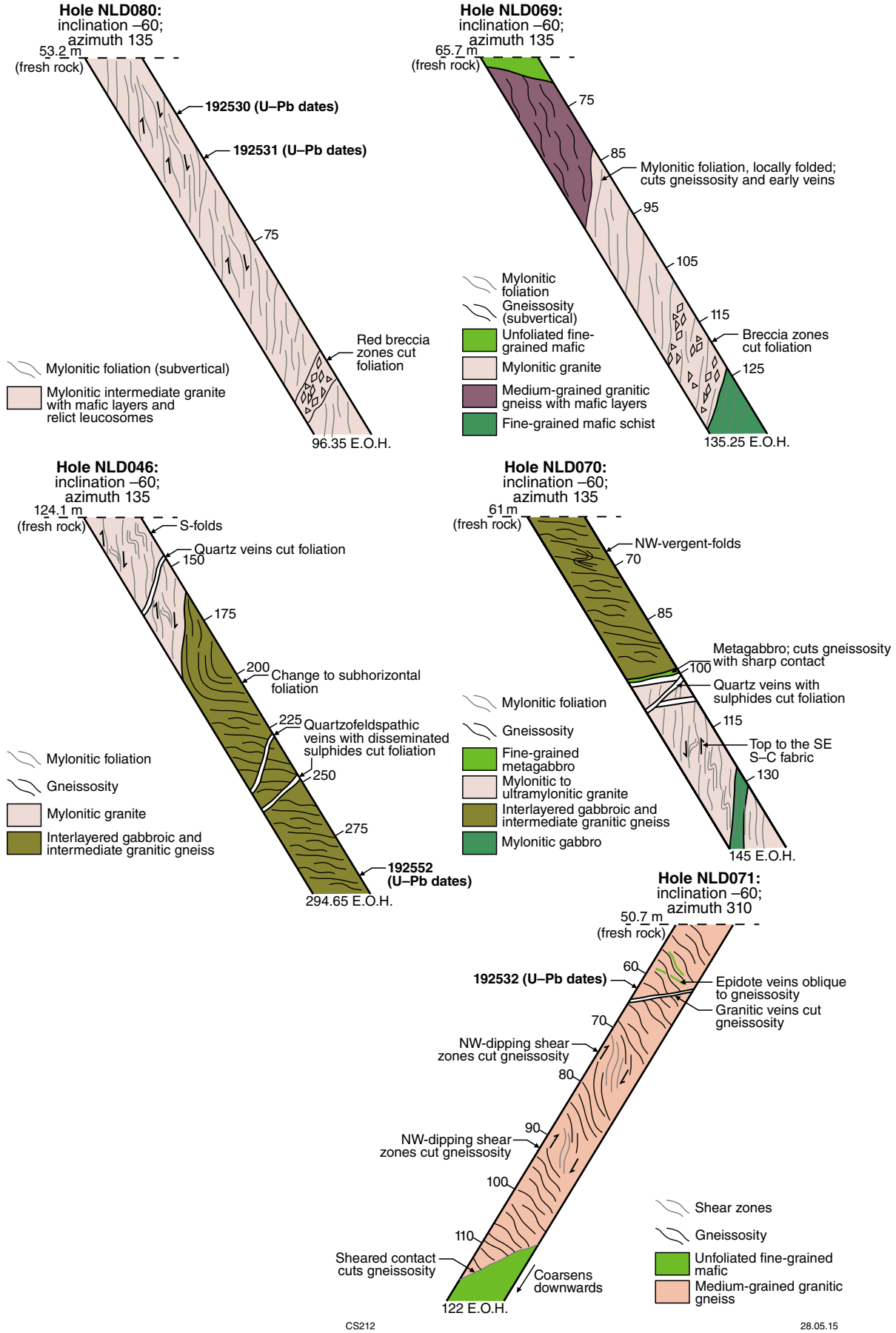

Figure 6. Schematic diagrams of the five diamond drillcores from the Atlantis Prospect, showing crosscutting relationships and locations of geochronology samples

The mylonite contains dark slaty layers rich in biotite and chlorite, blue quartz porphyroclasts, and disseminated sulfide minerals. The asymmetry of the porphyroclasts indicates dextral kinematics, but the mylonite is itself locally folded. Below about 111 m are a series of distinct breccia zones, up to 10 cm wide, which crosscut the mylonitic foliation. Thick quartz veins also cut the mylonite. Below about 125 m is a fine-grained, foliated mafic schist with disseminated sulfide minerals, locally interlayered with deformed granite, but also locally cut by granitic veins.

Drillcore NLD070

Drillcore NLD070 extends to a depth of 145.05 m (Fig. 6). The upper part and structurally highest section of the core is composed of interlayered granitic and gabbroic gneisses, all of which carry a subhorizontal to gently southeast-dipping foliation that is axially planar to tight, northwest-vergent, small-scale folds (Fig. 4b). The folded gneiss is cut by a dolerite intrusion with sharp contacts between about 96 and 98.7 m. A second dolerite that is possibly part of the same intrusion cuts the gneiss at 101.0 m, and contains fine quartz veins with pyrite, and disseminated sulfide minerals throughout. Structurally below the dolerite is a mostly vertical, but asymmetrically folded, mylonitic foliation, developed in granitic and locally mafic gneiss, similar to other core examples in the Atlantis prospect. The foliation defines dextral S–C fabrics indicating top to the southeast shear, although this fabric may be folded. The direction of movement is inferred from the long axes and alignment of minerals in the mylonitic foliation.

Analytical methods

U–Pb zircon geochronology

A detailed description of sample preparation and analytical details is provided by Wingate and Kirkland (2013), and summarized briefly below. Zircons were separated from each sample using standard magnetic and density techniques. The zircons, together with zircon reference standards, were cast in epoxy mounts, which were then polished to approximately half-grain thickness for analysis. Each mount was documented with transmitted and reflected light microphotographs and cathodoluminescence (CL) images. Measurements of U, Th, and Pb were conducted using the SHRIMP II ion microprobes in the John de Laeter Centre for Isotope Research at Curtin University. U–Th–Pb ratios and absolute abundances were determined relative to the BR266 standard zircon (559 Ma, 903 ppm ^{238}U; Stern, 2001), analyses of which were interspersed with those of unknown zircons. Fractionation of ^{207}Pb*/^{206}Pb* (Pb* = radiogenic Pb) was monitored during each session by analysis of the 3465 Ma OG1 zircon standard (Stern et al., 2009) and no fractionation correction was deemed necessary. Measured compositions were corrected for common Pb using non-radiogenic ^{204}Pb for all analyses. Prior to analysis, each site was cleaned by rastering the primary ion beam over the area for up to three minutes, and common Pb counts did not decrease during the analyses. In most cases, corrections are sufficiently small to be insensitive to the choice of common Pb composition, and an average crustal composition (Stacey and Kramers, 1975) appropriate to the age of the mineral was assumed.

Data were reduced using Squid, in-house macros, and Isoplot (Ludwig, 2003, 2009), using decay constants of Steiger and Jäger (1977). Calculated mean ages are quoted in the text with 95% uncertainties ($t\sigma\sqrt{MSWD}$; Ludwig, 2003) and the value of the mean square of weighted deviates (MSWD). For concordia ages (Ludwig, 1998), we quote the MSWD for combined concordance and equivalence, although in cases where the MSWD for either parameter is unacceptably high, we do not report the concordia age. In the descriptions of the results, and in Figure 7, analyses are placed into interpretative groups, including Group I (igneous crystallization), M (metamorphic granulite-facies zircon), M2 (second stage of metamorphism), X (inheritance), P (radiogenic-Pb loss), and D (excluded data).

Re–Os pyrite geochronology

The Re–Os geochronometer is based on the decay of ^{187}Re to ^{187}Os. The half-life of ^{187}Re is very long (c. 42 Ga) so the amount of radiogenic ^{187}Os is small, which creates analytical challenges. Re and Os are both siderophile and chalcophile elements, and have strong affinity for sulfide minerals. In many cases, the incorporation of both Re and Os into sulfide minerals necessitates the use of an isochron to attempt to remove the influence of non-radiogenic Os on the age information. Crustal rocks will rapidly develop elevated ^{187}Os/^{188}Os values because of high Re/Os ratios relative to the mantle, so that mantle-like Os initial ratios (^{187}Os/^{188}Os <0.13) are distinct from crust-like values (^{187}Os/^{188}Os >0.5; Chesley and Ruiz, 1998). Thus, the initial Os isotopic composition of the pyrite also constrains the nature of potential source region(s). However, some sulfide minerals in gold deposits contain very low Re concentrations, such that no or very little Os becomes incorporated into the sulfide mineral at its time of formation. Such sulfide minerals are termed low-level high-radiogenic (LLHR) and may provide an important method of constraining the timing of gold mineralization in the absence of associated molybdenite (which has relatively high Re content). This is because the Os in a LLHR, to a first approximation, can be assumed to have formed entirely from radiogenic decay. This method was used by Morelli et al. (2005) to date vein-style gold deposits in Nova Scotia using both pyrite and arsenopyrite.

A sample of pyrite (GSWA 192522) was extracted from a gold-bearing quartz vein in the 167.0 – 167.1 m depth interval of drillcore NLD210, and two fractions were analysed, one using a single spike, and the other using a double spike.

The Re and Os concentrations and isotope ratios in pyrite were determined using Carius tube, solvent extraction, anion chromatography, and isotope dilution thermal

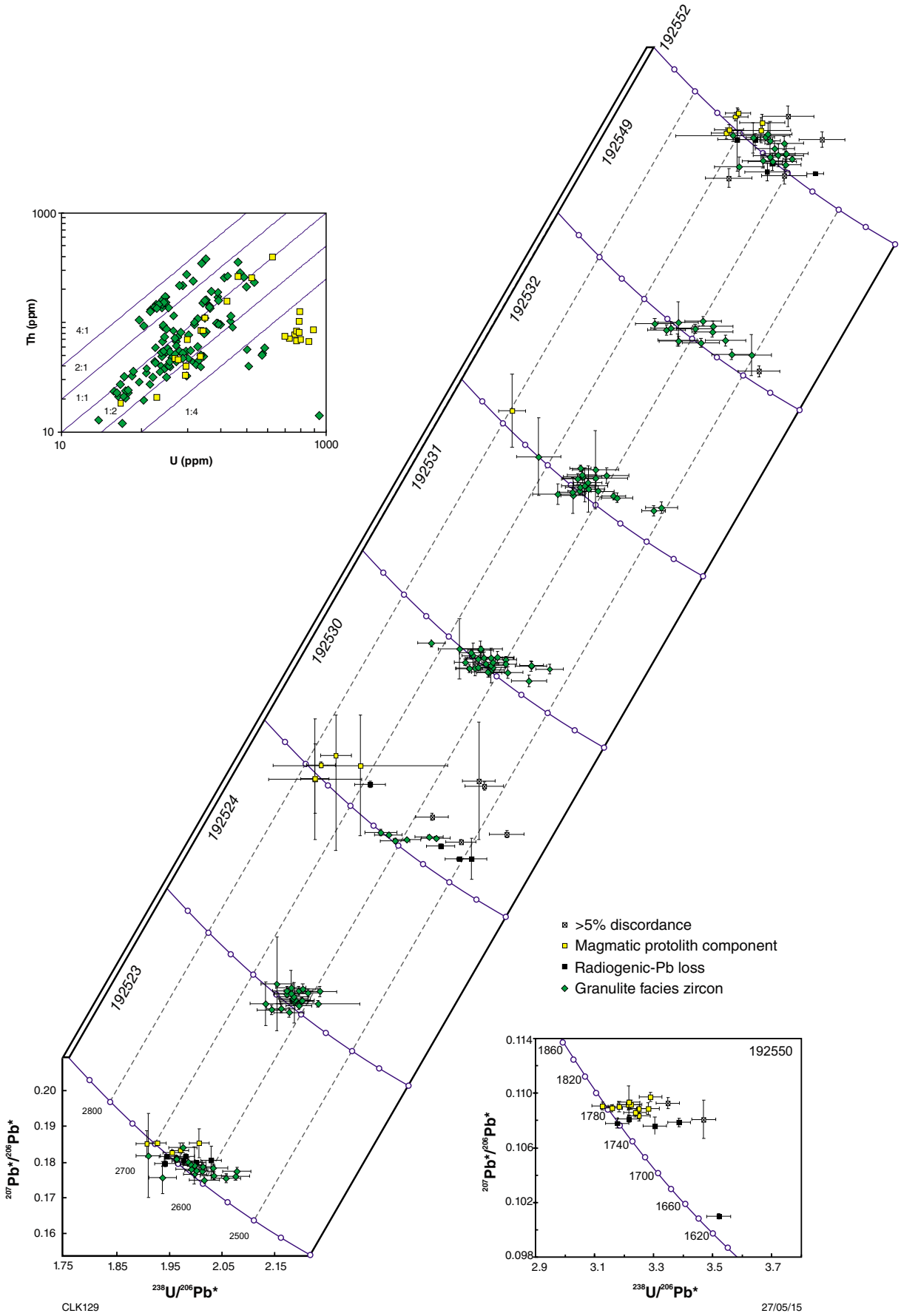

Figure 7. Stacked inverse concordia diagrams for Hercules Gneiss samples of the Tropicana Zone. Inset (upper), Th versus U plot for all zircon analyses; (lower) inverse concordia diagram for crosscutting Proterozoic intrusion sample

ionization mass spectrometry (IDTIMS) techniques. The method used in double spike analysis is described in detail by Selby and Creaser (2004). For this work, a mixed double spike containing known amounts of isotopically enriched ^{185}Re, ^{190}Os, and ^{188}Os analyte was used (Markey et al., 2007). Isotopic analysis was performed on a ThermoScientific Triton mass spectrometer by Faraday collector (Re) and secondary electron multiplier (Os). Total procedural blanks for Re and Os are less than 0.5 pg and 1 pg, respectively. These procedural blanks are insignificant in comparison to the Re and Os concentrations measured in this work. The Chinese molybdenite powder HLP-5 was routinely analysed and during the period of analysis returned a Re–Os date of 221 ± 1 Ma identical to that reported by Markey et al. (1998). In addition, the age determined for the Henderson Molybdenite Reference Material RM8599, using the above methods and instrumentation, was 27.71 ± 0.13 Ma, in accord with previous determinations (Markey et al., 2007).

Whole-rock geochemistry

Major element oxides and selected trace elements were determined by X-ray fluorescence (XRF). Other trace elements and rare earth elements (REE) were measured by inductively coupled plasma mass spectrometry (ICPMS; Morris, 2000, 2007). Based on multiple analyses of in-house reference materials and duplicate samples, precision and accuracy of major elements and trace elements by XRF is estimated at better than 4% relative standard deviation (RSD). Trace elements and REE by ICPMS are better than 5% RSD in most cases. Further details of the geochemistry standards for the samples in this work are provided in the GSWA online geochemistry database (www.dmp.wa.gov.au/geochem).

Results

U–Pb geochronology of drillcore samples in the Tropicana Zone

In the following section we report the results of SIMS (SHRIMP) U–Pb geochronology of zircon crystals extracted from drillcore samples in the Neale Project area, Tropicana Zone. GSWA geochronology records with U–Pb data tables are listed in Table 1 and available online at <www.dmp.wa.gov.au/geochron/>. A stacked concordia plot is provided in Figure 7, representative CL images in Figure 8, and an age histogram in Figure 9. All drillcore samples, excluding GSWA 192550 from a late microgranite vein, contain a component of near-spherical multifaceted zircon grains consistent with formation during high-pressure metamorphism (Hoskin and Black, 2000). There is considerable debate about the interpretation of U–Pb zircon dates from granulite-facies meta-igneous rocks, reflecting the wide variety of growth and/or alteration processes that may have affected zircons in such rocks. In granulite-grade rocks, zircon growth and alteration processes range from solid-state recrystallization of protolith zircon, on the basis of preserved primary zonation in recrystallized zircon domains (Hoskin and Black, 2000), to precipitation of new zircon from melt during the retrograde metamorphic stage (Roberts and Finger, 1997). A combination of these mechanisms may occur at essentially the same time to produce an apparent continuum of U–Pb dates. Due to granulite-facies overprinting, the preservation of primary magmatic crystallization ages may be limited.

We apply the following consistent approach in the interpretation of the U–Pb geochronology from these samples. Zircon cores preserving textural evidence of forming during igneous crystallization within a viscous felsic melt, such as fine oscillatory zoning are assigned to:

- Group I: analyses that make up the oldest statistically coherent age component, which may reflect the crystallization age of protolith components within the gneiss, provided no effects of radiogenic-Pb loss can be diagnosed.
- Group P: analyses yielding younger dates may indicate zircons that have undergone radiogenic-Pb loss, which may also be indicated by measured high U and Th contents, which lead to radiation damage and enhanced calculated alpha radiation doses or reduced grain densities.
- Group M: zircon rims and entire crystals that preserve textural evidence of growth during fluid-present, granulite-facies metamorphism or metasomatism, including broad concentric and sector zoning, homogeneous domains, and subspherical to spherical crystal forms (e.g. Flowers et al., 2010; Smithies et al., 2011; Tichomirowa et al., 2005). Because granulite-facies metamorphic processes can be prolonged (Smithies et al., 2011), we provide both the range of ^{207}Pb*/^{206}Pb* dates for Group M and also calculate the youngest statistically coherent group. The youngest age component in Group M provides a conservative estimate for the latest phase of granulite-facies zircon growth within the sample.

Drillcore NLD210 — Hercules prospect

GSWA 192523: diorite to quartz monzodiorite gneiss

Sample GSWA 192523 is a diorite gneiss recovered from 143.90 – 144.05 m depth. The gneiss consists of about 60% sericitized anhedral fine- to medium-grained plagioclase and 25% fine-grained, recrystallized aggregates of anhedral green amphibole. Interstitial bands and lenses of microcrystalline quartz form about 10% of the rock. Feldspar crystals are commonly crosscut by veinlets of sericite and carbonate. Minor phases include ilmenite altered to titanite, as well as leucoxene, epidote, chlorite, and zircon. Minor shear fractures through the rock consist of microcrystalline quartz and amphibole. In thin section, the rock is classified as a hydrothermally altered quartz-bearing amphibolite, likely originally derived from a quartz diorite, as suggested by the

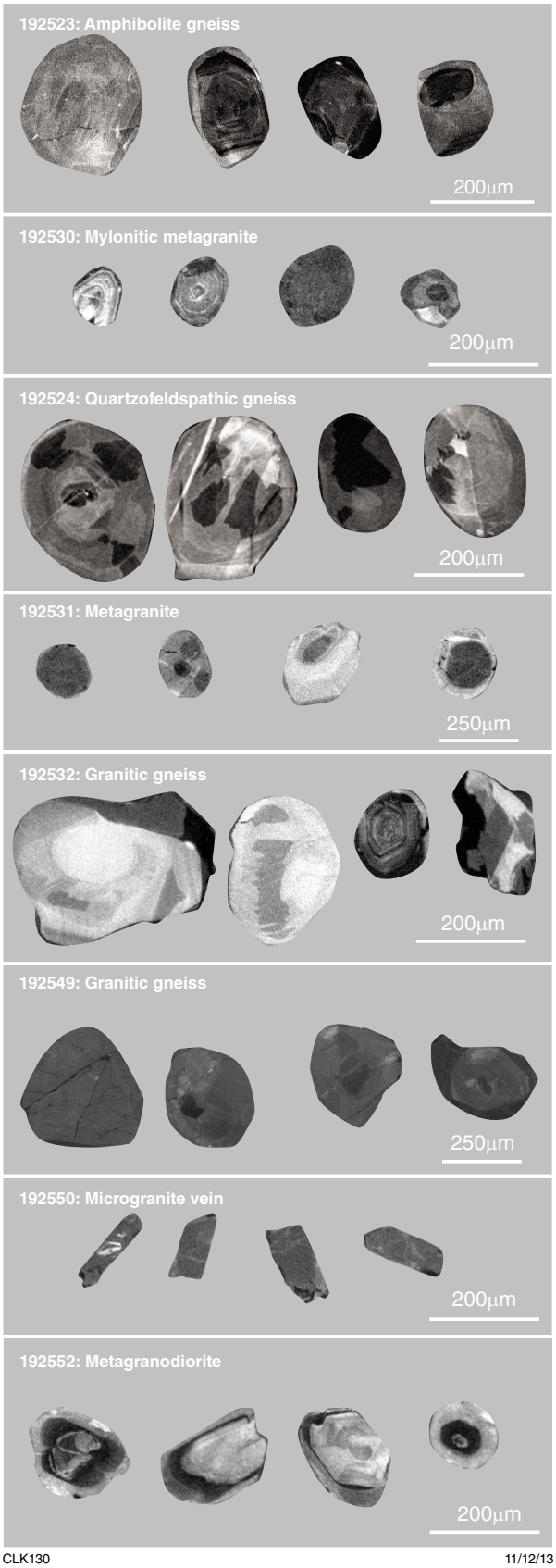

Figure 8. **Representative cathodoluminescence (CL) images of zircons from drillcore samples in the Hercules Gneiss, Tropicana Zone. Note the distinctly different zircon crystal morphology for GSWA 192550, microgranite vein.**

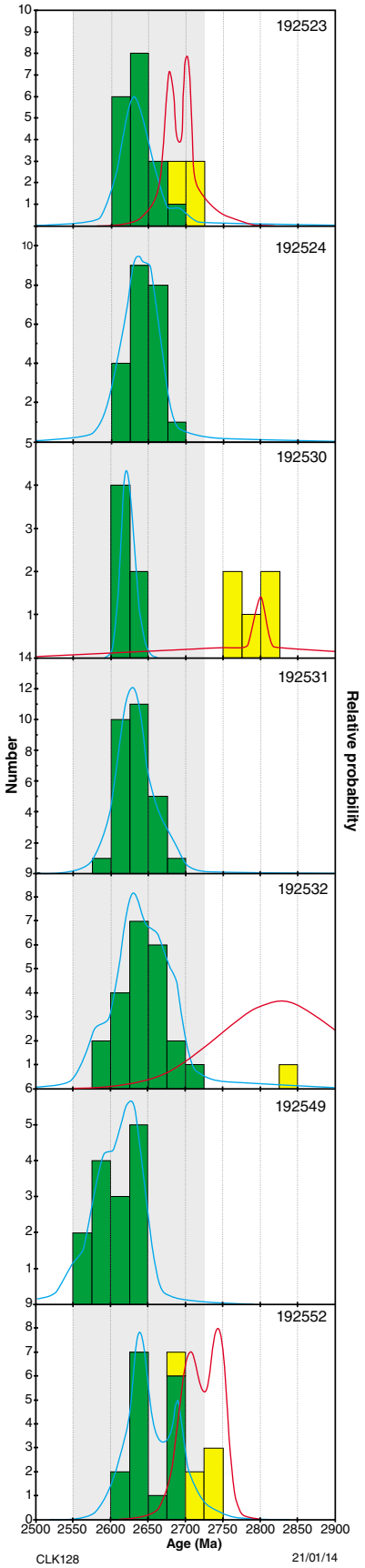

Figure 9. **Stacked histograms of zircon ages in the Hercules Gneiss. Green fill indicates granulite-facies zircon growth. Yellow fill indicates igneous crystallization or an inherited component within the protolith.**

preservation of igneous feldspar microlites. The inferred paragenetic sequence is: plagioclase, amphibole, quartz, chlorite, epidote, sericite. Formation of shear zones containing amphibole occurred during amphibolite-facies metamorphism. Zircons extracted from this sample are colourless to dark brown, anhedral to subhedral, and strongly rounded. The crystals are up to 300 μm long, and equant to slightly elongate, with aspect ratios up to 4:1. In CL images, the crystals consist of concentrically zoned cores, overgrown by one or more generations of zircon rims, most of which display broad concentric zoning, sector zoning, or are internally homogeneous.

Five analyses of five zircon cores (Group I) yield a weighted mean $^{207}Pb^*/^{206}Pb^*$ date of 2692 ± 16 Ma (MSWD = 2.4), interpreted as the magmatic crystallization age of the igneous protolith of the gneiss. These analyses indicate mainly moderate uranium concentrations (median 213 ppm) and Th/U ratios (median 0.98). Seven analyses of seven zircon cores (Group P), yield $^{207}Pb^*/^{206}Pb^*$ dates of 2669–2650 Ma, interpreted to reflect minor ancient loss of radiogenic Pb from protolith zircons. Group P analyses indicate mainly low uranium concentrations (median 155 ppm) and moderate Th/U ratios (median 0.79). Eighteen analyses of 18 zircon rims (Group M1) yield $^{207}Pb^*/^{206}Pb^*$ dates of 2690–2608 Ma, interpreted to reflect the timing of granulite-facies metamorphism. Group M analyses indicate mainly low uranium concentrations (median 73 ppm) and moderate Th/U ratios (median 0.64). One analysis of an outermost zircon rim (Group M2), yields a $^{207}Pb^*/^{206}Pb^*$ date of 1770 ± 23 Ma (1σ). This analysis indicates a low uranium concentration (51 ppm) and very low Th/U ratio (0.01). The date of c. 1770 Ma is interpreted as the age of metamorphism causing new zircon rim growth.

The concentric zoning and elongate (prismatic) shapes of zircon cores in Groups I and P are typical of zircons formed during igneous crystallization within a viscous felsic (granitic) melt, whereas the very broad concentric and sector zoning within, and subspherical shapes imparted by, zircon rims in Group M are characteristic of zircons formed during fluid-rich, granulite-facies metamorphism or metasomatism (e.g. Flowers et al., 2010). Within the results for Group M, the 15 youngest analyses yield a weighted mean $^{207}Pb^*/^{206}Pb^*$ date of 2632 ± 7 Ma (MSWD = 1.7), interpreted as a conservative estimate for the youngest phase of granulite-facies zircon growth.

GSWA 192524: diorite to quartz diorite gneiss

Sample GSWA 192524 was recovered from the upper quartzofeldspathic orthogneiss at a depth of 59.95 to 60.20 m (Fig. 5). The sample consists of a strongly foliated matrix dominated by microcrystalline aggregates of quartz and feldspar and quartz–sericite intercalated with folia of microcrystalline muscovite and sericite. The sample contains about 60% microcrystalline quartz–feldspar mosaic, 30% sericite, 5% epidote, and minor iron–titanium oxide minerals, calcite, and zircon. The microcrystalline assemblages engulf quartz–feldspar augen containing relict medium-grained anhedral albite-twinned plagioclase (andesine, An_{34}). Plagioclase is either unaltered or clouded by cryptocrystalline to microcrystalline saussurite and epidote. The presence of relict plagioclase indicates derivation of the gneiss from an igneous rock of intermediate composition, possibly quartz diorite. Penetrative deformation of the parent rock resulted in interlayering of quartz–feldspar mosaic with sericite-rich bands. Zircons isolated from this sample are colourless to dark brown, and mainly anhedral and strongly rounded. The crystals are up to 400 μm long, and generally equant. In CL images, most crystals display broad concentric or sector zoning. Some zircons contain very small cores, which may represent vestigial protolith crystals, although these were below the spatial resolution of the ion beam.

Twenty-two analyses of 20 zircons (Group M) yield $^{207}Pb^*/^{206}Pb^*$ dates of 2677–2603 Ma, interpreted as the timing of granulite-grade metamorphism and zircon growth, consistent with the distinctive CL response and spherical form of the zircons. All analyses indicate mainly low U concentrations (42–122 ppm) and moderate Th concentrations (94–382 ppm). Their uniform appearance and uniformly high Th/U ratios (2.22 – 3.25) suggest that all zircons had a similar origin. Within the results for Group M, the 17 youngest analyses yield a weighted mean $^{207}Pb^*/^{206}Pb^*$ date of 2634 ± 8 Ma (MSWD = 1.9), which provides a conservative estimate for the youngest phase of granulite-facies zircon growth.

Drillcore NLD097 — Hercules prospect

GSWA 192549: monzodiorite to quartz monzodiorite gneiss

Sample GSWA 192549 was recovered from 139.12 – 139.44 m depth. Based on whole-rock chemistry, a CIPW norm suggests that under equilibrium conditions this rock would contain 28% albite, 14% anorthite, 24% quartz, 9% orthoclase, 11% biotite, 5% hematite, 3% corundum, and accessory ilmenite, and apatite, with a norm total of 97%, and a chemical index of alteration of 63/100 (Nesbitt and Young, 1982). Similar fresh material elsewhere in this drillcore contains about 40% quartz, 35% K-feldspar, 22% plagioclase, 1% biotite, and accessory muscovite, chlorite, zircon, rutile, titanite, monazite, ilmenite, and apatite. The rock is equigranular and has a granoblastic texture. Quartz displays undulose extinction and feldspar shows both microcline and microperthitic orthoclase exsolution. Biotite grains display a prominent sagenite texture of exsolved orientated rutile needles. Zircons from this sample are colourless to pale brown, anhedral and strongly rounded. The crystals are up to 300 μm long, and equant, with aspect ratios up to 4:1. In CL images, the crystals reveal broad concentric zoning, sector zoning, or are internally homogeneous. Homogeneous, high-uranium overgrowths mantle some crystals. The broad concentric and sector zoning, subspherical crystal forms, and homogeneous overgrowths are characteristic of zircons formed during granulite-facies conditions (e.g. Flowers et al., 2010).

Two analyses >5% discordant and one analysis that touched a fracture (Group D) are not considered further.

Fourteen analyses (Group M) yield $^{207}Pb^*/^{206}Pb^*$ dates of 2644–2554 Ma, interpreted as the age of granulite-facies zircon growth. These analyses indicate mainly low uranium concentrations (median 59 ppm), low thorium concentrations (median 61 ppm) and moderate Th/U ratios (median 1.01). Within the results for Group M, the seven youngest analyses yield a weighted mean $^{207}Pb^*/^{206}Pb^*$ date of 2589 ± 18 Ma (MSWD = 1.7), which provides a conservative estimate for the youngest phase of granulite-facies zircon growth.

GSWA 192550: monzogranite vein

Sample GSWA 192550 is a microgranite vein sampled from 121.34 – 121.44 m depth. The vein crosscuts granitic gneiss (sample GSWA 192549) in the same core. The sample is composed of about 50% quartz, 40% plagioclase, 8% K-feldspar, 1% muscovite, and accessory zircon, epidote, and apatite. The rock has a granoblastic texture and does not exhibit a pervasive deformation fabric. Quartz displays undulose extinction and feldspar is extensively altered by sericite clouding. This sample yielded colourless to brown, subhedral to euhedral zircons with aspect ratios up to 5:1. The crystals exhibit low CL response and are mainly homogeneous, although several show faint indications of apparently older cores.

Two analyses >5% discordant (Group D) are not considered further. Eleven analyses (Group I) yield a weighted mean $^{207}Pb^*/^{206}Pb^*$ date of 1783 ± 3 Ma (MSWD = 1.12), interpreted as the magmatic crystallization age of the microgranite vein. Five analyses (Group P) yield $^{207}Pb^*/^{206}Pb^*$ dates of 1745–1612 Ma, interpreted to reflect minor ancient radiogenic-Pb loss, consistent with high uranium contents, and a lower calculated grain density for Group P (median 4.31 g/cc) compared to Group I (4.37 g/cc).

Drillcore NLD080 — Atlantis prospect

GSWA 192530: mylonitic metagranite

Sample GSWA 192530, recovered from 60.2 – 60.3 m depth, is a fine-grained mylonitic, augen-metagranite. The rock consists of about 20% porphyroclasts and 80% fine-grained recrystallized matrix. The majority of porphyroclasts are quartz with recrystallized mantles or strain shadows of fine quartz. The matrix consists of quartz, biotite, chlorite, muscovite, rutile, pyrite, ilmenite, zircon, and monazite. Biotite occurs as rare subhedral phenocrysts up to 1.6 mm long. Chlorite replaces biotite and pseudomorphs other grains. Fine-grained muscovite is xenoblastic to subidioblastic. Short-wave infrared (SWIR) spectra indicate the presence of a phengitic component in the mica. Rutile is an accessory phase and appears to have replaced ilmenite. Pyrite occurs as disseminated rounded crystals up to 20 µm across and also as inclusions within quartz. Zircon is associated with biotite and rutile in the matrix. Rare monazite, up to 15 µm across, is interpreted as a very late-crystallized phase, occupying interstices associated with chlorite cleavage planes and fractures in quartz. Monazite typically appears in clusters of infilling grains, associated with chlorite and fine-grained muscovite. Zircons are subhedral, brown, and strongly rounded to subspherical. The crystals are up to 400 µm across, and equant. In CL images, most crystals consist of concentrically zoned cores, overgrown by zircon rims that exhibit broad concentric or sector zoning or are internally featureless. Six analyses are >5% discordant, and are considered not to be geologically significant.

Five analyses (Group I) yield a concordia age of 2795 ± 12 Ma (MSWD = 0.66), interpreted as the magmatic crystallization age of the granite or of a protolith component within this rock. These analyses were located on low-uranium, zoned zircon cores. One core analysis yields a $^{207}Pb^*/^{206}Pb^*$ date of 2755 ± 7 Ma, is 1% outside two-sigma analytical uncertainty of concordia, and is interpreted to have lost radiogenic Pb. Ten analyses (Group M) yield $^{207}Pb^*/^{206}Pb^*$ dates of 2636–2566 Ma, interpreted as the time of granulite-facies metamorphism and zircon growth, consistent with their CL textures and crystal forms. Six analyses with statistically coherent ages in Group M yield a weighted mean of 2623 ± 7 Ma (MSWD = 1.7), interpreted as the age of peak granulite-facies zircon growth. These analyses are located on zircons that are either internally homogeneous, or display broad concentric and sector zoning in CL images; these textures, together with their subspherical shapes, are characteristic of growth during granulite-grade metamorphism (e.g. Flowers et al., 2010).

GSWA 192531: mylonitic metagranite

Sample GSWA 192531 was recovered from the 68.35 – 68.50 m depth. Similar material from this drillcore in thin section displays a strong mylonitic foliation and two subordinate sets of shear bands producing an anastomosing fabric. The rock consists of about 60–70% quartz, 15% phengitic muscovite, 5% biotite, 5% chlorite, and 5% dolomite, with accessory amphibole (gedrite), ilmenite, pyrite, rutile, and zircon. Quartz is recrystallized and also occurs as porphyroclasts. Fine-grained muscovite replaces biotite and is in turn replaced by chlorite. Muscovite aggregates define mica fish, C, and C' shear bands. Two generations of biotite are recognized; a late high-Mg phase forming cleavage domains, and an early subidioblastic phase. Zircons from this sample are pale brown to black and anhedral to subhedral and strongly rounded. The crystals are up to 250 µm long, and equant, with aspect ratios up to 3:1. In CL images, the crystals reveal broad concentric zoning, sector zoning, or are internally homogeneous. Some zircons contain very small, apparently vestigial cores, which are high in uranium and below the spatial resolution of the ion beam. Fractures radiate outwards from these cores and penetrate into the surrounding zircon.

Twenty-eight analyses of 17 zircons are concordant to slightly discordant (only three analyses are outside two-sigma analytical uncertainty of concordia) and yield $^{207}Pb^*/^{206}Pb^*$ dates of 2683–2585 Ma that are dispersed beyond analytical precision. However, there is no systematic relationship between apparent age and location within the crystals. Of 11 analysis pairs of inner and outer parts of the same zircons (i.e. possible cores and rims), only one pair indicated that the rim was significantly

younger than the core, and one other indicated the rim was significantly older than the core. The remaining nine analysis pairs indicated no significant or systematic difference in apparent age between cores and rims. Similarly, no relationship exists between U, Th, or Th/U and locations within the crystals. We interpret the CL textures, grain shapes, and U–Pb systematics as indicative of granulite-grade zircon growth throughout the interval defined by the $^{207}Pb^*/^{206}Pb^*$ dates of 2683–2585 Ma (Group M). Within the results for Group M, the 18 youngest analyses yield a weighted mean $^{207}Pb^*/^{206}Pb^*$ date of 2624 ± 6 Ma (MSWD = 1.3), which provides a conservative estimate for the youngest period of high-grade metamorphism.

Drillcore NLD071 — Atlantis prospect

GSWA 192532: granitic gneiss

Sample GSWA 192532 was recovered from 63.8 – 64.1 m depth. Granitic gneiss in this drillcore consists of about 40–45% K-feldspar, 30% quartz, 20% plagioclase, 5% biotite, and accessory zircon, apatite, pyrite, ilmenite, muscovite, chlorite, biotite, amphibole (gedrite), Fe-oxide, actinolite–tremolite, gold, and epidote. The rock is interpreted as a granitic gneiss overprinted by muscovite and chlorite alteration. Gold occurs as subhedral (truncated tetrahedral) grains, up to about 10 µm across, that adjoin K-feldspar and Fe-oxide minerals (after pyrite). Gold is interpreted to have developed within a Fe-oxide-filled fracture that is orthogonal to shear bands. Zircons are colourless to black, anhedral to subhedral, and rounded. Many are angular broken grain fragments. The crystals are up to 250 µm long, and equant to elongate, with aspect ratios up to 5:1. In CL images, the crystals consist of concentrically zoned cores, overgrown by one or more generations of zircon rims, most of which display broad concentric zoning, sector zoning, or are internally homogeneous. Some zircons do not contain cores and are sector zoned or homogeneous.

Four analyses are >5% discordant (Group D). One analysis of a zircon core (Group I), yields a $^{207}Pb^*/^{206}Pb^*$ date of 2826 ± 83 Ma (1σ), interpreted as the age of magmatic crystallization of the igneous protolith of the gneiss. The concentric zoning and elongate (prismatic) shape of this zircon core is consistent with growth during igneous crystallization within a viscous felsic (granitic) melt. This analysis indicates a moderate uranium concentration (86 ppm) and a moderate Th/U ratio (0.48). Other analysed cores are discordant (Group D). Twenty-two analyses of 16 zircon rims and discrete crystals (Group M) yield $^{207}Pb^*/^{206}Pb^*$ dates of 2718–2580 Ma, interpreted to indicate the time of granulite-facies metamorphism. These analyses indicate mainly low uranium concentrations (median 81 ppm) and moderate Th/U ratios (median 0.66). The broad concentric and sector zoning within, and subspherical shapes produced by, the zircon rims and the discrete homogeneous grains in Group M are characteristic of zircons formed during granulite-facies metamorphism (e.g. Flowers et al., 2010). Within the results for Group M, the seven youngest analyses yield a weighted mean $^{207}Pb^*/^{206}Pb^*$ date of 2611 ± 17 Ma (MSWD = 1.8), which provides a conservative estimate for the latest phase of granulite-facies zircon growth.

Drillcore NLD046 — Atlantis prospect

GSWA 192552: monzodiorite to quartz monzodiorite gneiss

Sample GSWA 192552 was recovered from 289.6 – 289.9 m depth. Based on the whole-rock chemistry, a CIPW norm suggests that under equilibrium conditions this rock would contain 30% albite, 22% anorthite, 19% quartz, 12% orthoclase, 3% hematite, 7% biotite, and accessory corundum, ilmenite, and apatite, with a norm total of 97%. Zircons from this sample are subhedral, colourless to brown, and rounded. The crystals are up to 250 µm long, and equant to elongate, with aspect ratios up to 5:1. In CL images, the crystals consist of concentrically zoned cores, overgrown by one or more generations of zircon rims, most of which display broad concentric zoning, sector zoning, or are internally homogeneous. Generally, low-uranium oscillatory-zoned cores are overgrown by inner high-uranium rims, which in turn are mantled by outer low-uranium rims. Some cores exhibit irregular outlines that may indicate corrosion or partial resorption.

Three analyses are >5% discordant and one analysis included a fracture; these four analyses (Group D) are not considered further. Six analyses of zircon cores (Group I) yield a concordia age of 2726 ± 14 Ma (MSWD = 1.7), interpreted as the age of magmatic crystallization of the monzodiorite protolith or of an inherited component within that protolith. These analyses indicate mainly low uranium concentrations (median 73 ppm) and moderate Th/U ratios (median 0.69). Five analyses of five zircon cores (Group P), yield $^{207}Pb^*/^{206}Pb^*$ dates of 2685–2598 Ma, interpreted to reflect minor radiogenic-Pb loss. The concentric zoning and elongate (prismatic) shapes of zircon cores in Groups I and P are typical of zircons formed during igneous crystallization within a viscous felsic magma. Sixteen analyses of zircon rims (Group M) yield $^{207}Pb^*/^{206}Pb^*$ dates of 2698–2615 Ma. These dates are dispersed beyond analytical precision, suggesting that they reflect prolonged zircon growth during high-grade conditions, consistent with their CL textures and subspherical shapes (e.g. Flowers et al., 2010). Within the results for Group M, the 13 youngest analyses yield a weighted mean $^{207}Pb^*/^{206}Pb^*$ date of 2641 ± 8 Ma (MSWD = 1.2), which provides a conservative estimate for the latest phase of granulite-facies zircon growth.

Geochemistry of Archean metagranites in the Tropicana Zone

The Biranup Zone contains several outcrops of Archean granites that have escaped Proterozoic remelting. These, together with Archean granites of the Northern Foreland, have distinctive major and trace element

compositions expected for Archean granites of the tonalite–trondhjemite–granodiorite (TTG) or transitional TTG series (e.g. Champion and Smithies, 2007), including high Na_2O, Al_2O_3, Sr, and Ba, and low K_2O and Yb concentrations (Fig. 10). Such granites are also rich in silica, with SiO_2 typically >70 wt%.

In contrast, the Archean granites of the Hercules Gneiss (Neale Project area, Tropicana Zone), all have dioritic to quartz-monzodioritic compositions, with a very narrow range of low silica values, from 58 to 64 wt%. Two broad compositional groups can be recognized based on major element variations (Fig. 10). The first is characterized by unusually high concentrations of MgO (to 5.27 wt%), Cr (to 270 ppm), and Ni (120 ppm). The second shows strong depletions in CaO, down to concentrations as low as 0.18 wt%, possibly correlated with depletions in Na_2O and enrichments in Fe_2O_3 and K_2O and clearly reflecting pervasive plagioclase-destructive alteration. Despite this alteration, it is most likely that all granitic rocks of the Hercules Gneiss belong to a single geochemical series, distinct from typical Archean felsic rocks. Many silicate alteration minerals (e.g. muscovite, chlorite, clinozoisite–epidote) in the Hercules Gneiss are enriched in Cr, Ni, and Ba (mostly <0.5 wt%) consistent with a protolith also enriched in these elements.

Archean granites similar in composition to the Hercules Gneiss granites form a rare but distinctive component of many Archean cratons, and are referred to as sanukitoids (e.g. Stern et al., 1989). Distinct from the silicic and low-$Mg^{\#}$ rocks of the TTG series, sanukitoids are defined as having $Mg^{\#}$~60, Cr ~200 ppm, Ni ~100 ppm, and high (>500 ppm) concentrations of both Sr and Ba at silica levels of about 60 wt% (e.g. Stern et al., 1989) (Fig. 11). The high-$Mg^{\#}$ and Cr and Ni concentrations reflect equilibration with mantle peridotite and, together with the LILE-enrichments, are widely regarded as reflecting direct derivation from a mantle source previously enriched through interaction with a subducted-slab-derived partial melt (Shirey and Hanson, 1984; Stern et al., 1989; Smithies and Champion, 2000; Martin et al., 2005).

Re–Os pyrite geochronology of drillcore samples from the Hercules Gneiss

A sample of pyrite (GSWA 192522) was extracted from a gold-bearing quartz vein from 167.0 – 167.1 m depth in drillcore NLD210, and two fractions were analysed, the first using a single spike, and the second using a double spike (Table 2). The first fraction indicated 3 ppb Re and a total Os content of 74 ppt, with a high $^{187}Re/^{188}Os$ ratio of >170,000, corresponding to a model age of 2107 ± 30 Ma (Os initial = 0.5). However, the use of a single spike does not provide a means to correct for mass fractionation during isotopic measurement of geological samples containing highly radiogenic Os (i.e. LLHR). The use of a double spike, which combines isotopically enriched ^{188}Os and ^{190}Os, permits both fractionation correction, and a more reliable determination of common Os. The second split of 192552 was double-spiked, and returned

Table 2. N-TIMS Re–Os isotopic composition of GSWA 192522 pyrite, Hercules Gneiss

Re (ppb)	± 2σ	*Total Os ppt*	± 2σ	$^{187}Re/^{188}Os$	± 2σ	$^{187}Os/^{188}Os$	± 2σ	ρ	*% ^{187}Re blank*	*% ^{187}Os blank*	*% ^{188}Os blank*	*Model Age (Ma)**	± 2σ
single spike													
3.259	0.014	74.1	45.6	17492	7692	625	275	0.999	0.08	0.02	44	2107	30
Re (ppb)	± 2σ	*^{187}Re (ppb)*	± 2σ	*^{187}Os (ppb)*	± 2σ	*Os pg*	*Model Age (Ma)**	± 2σ					
double spike													
4.238	0.02	2664	13	94.23	0.75	2171.3	2087	21					

NOTES: All uncertainites are reported at the two sigma level; all data are blank corrected, blanks for Re and Os were <0.5 and <1 pg, respectively. All uncertainities are determined through the full propagation of uncertainties of the Re and Os mass spectrometer measurements, blank abundances and isotopic compositions, spike calibrations, and reproducibility of standard Re and Os isotopic values; ρ (rho) is the error correlation.
* Model age determined using an initial $^{187}Os/^{188}Os$ value of 0.5.

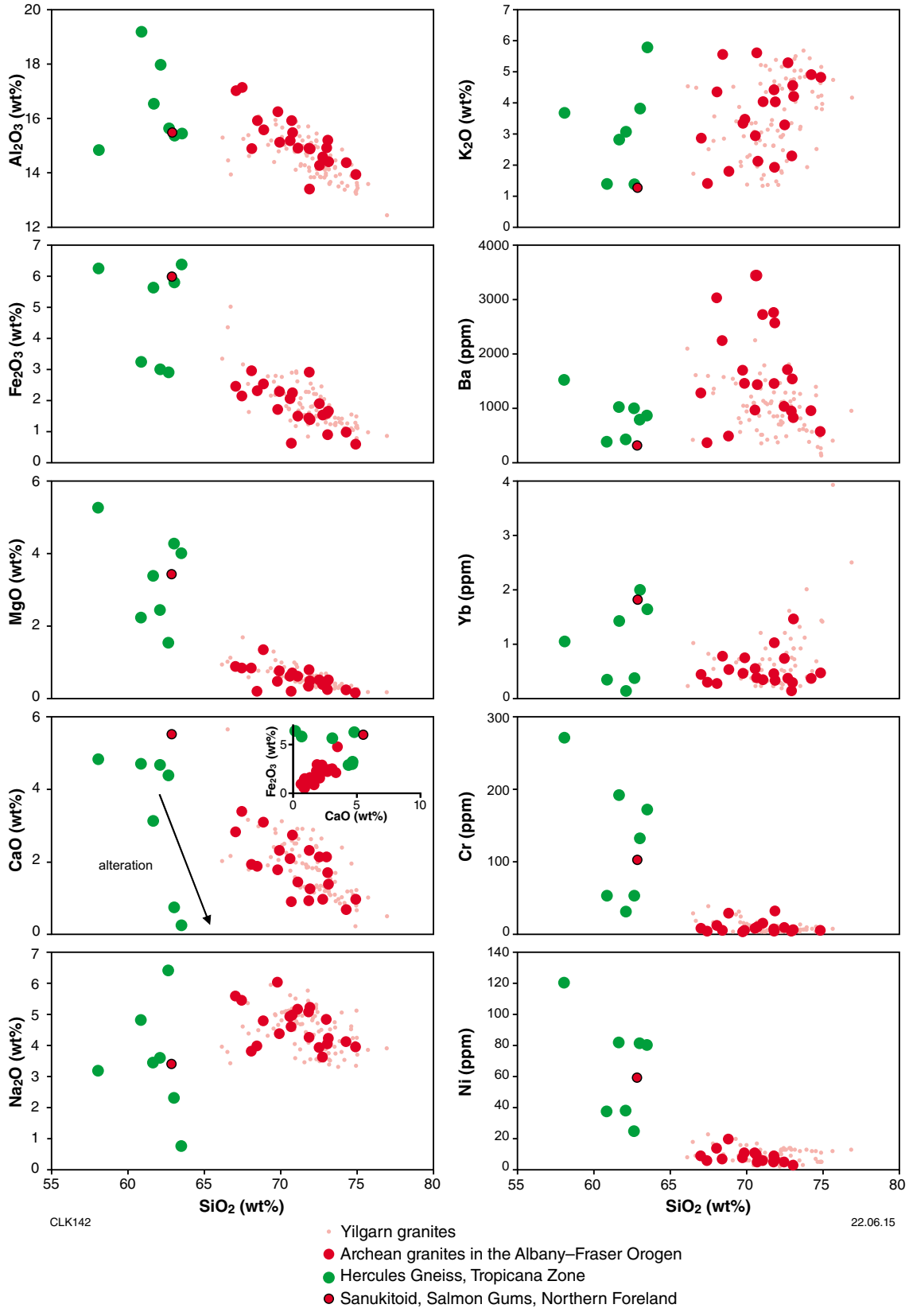

Figure 10. Compositional variation plots of major and trace elements versus SiO_2 (Harker diagrams), with inset of iron versus calcium for the Hercules Gniess, Tropicana Zone, in comparision to other proximal granitoids

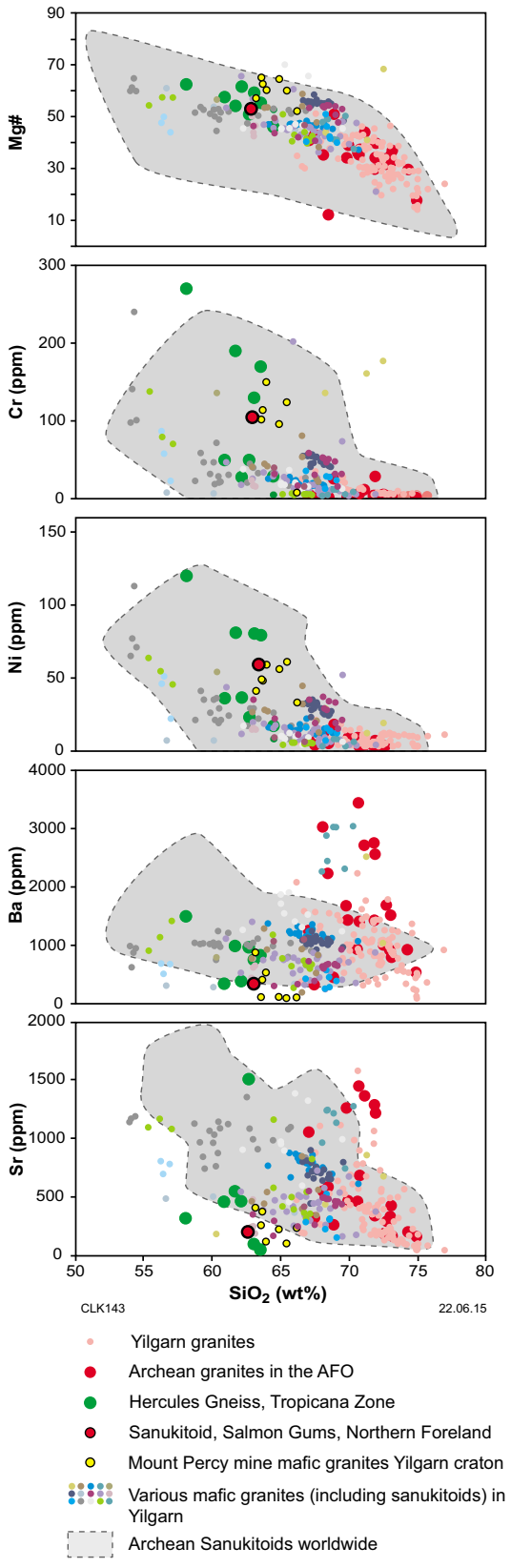

Figure 11. Compositional variation plots of major elements versus SiO_2 (Harker diagrams) of Hercules Gneiss drillcore samples in comparison to other Archean granites. Note elevated Mg, Cr, Ni, Sr, and Ba at SiO_2 = c. 60 wt% in the Hercules Gneiss are indicative of sanukitoid compositions.

4.2 ppm of total Re and 94 ppb of radiogenic ^{187}Os (out of 2.2 ng of common Os). The elevated amount of common Os means the calculated model age is sensitive to the choice of isotopic composition of initial $^{187}Os/^{188}Os$. Assuming an initial value of 0.5 ppt Os yields a model age of 2087 ± 21 Ma. Using a mantle value increases the model age to 2093 Ma and a more crustal value of 1 ppt Os results in a model age of 2079 Ma. In all cases, the model ages are within uncertainty of the single-spike determination. We interpret the age of pyrite growth to be c. 2100 Ma.

Discussion

Geochemistry of Archean rocks in the Tropicana Zone: Hercules Gneiss

In the Yilgarn Craton, a rare class of low-Si granites has been referred to as 'mafic granites' (e.g. Champion and Sheraton, 1997) and includes variably LILE-enriched groups of sanukitoids and sanukitoid-like rocks typically emplaced around 2655 Ma. In Figure 11, the sanukitoids of the Hercules Gneiss are compared with the various 'mafic granite' bodies from throughout the Yilgarn Craton (data from David Champion; written comm., 2014) and with sanukitoids from other Archean cratons worldwide (data from Smithies and Champion, 2000; GEOROCK database <http://georoc.mpch-mainz.gwdg.de/>). The sanukitoids from the Neale Project area clearly fall within the global sanukitoid field (Fig. 11). Along with the distinctive compositions of sanukitoids, the rarity of these rocks within any Archean craton provides additional evidence that the granite protoliths of the Hercules Gneiss represent a single suite of rocks intruded more or less at the same time.

In other Archean cratons, sanukitoids have been shown to have intruded late in the magmatic history, often several tens of Ma after the cessation of TTG magmatism (e.g. Stern et al., 1989; Evans and Hanson, 1997; Smithies and Champion, 2000), possibly reflecting remobilization of the subduction-modified source through processes such as slab breakoff (e.g. Van Kranendonk et al., 2007). The intrusions are typically localized along major structures interpreted as, or related to, crustal-scale sutures (e.g. Smithies and Champion, 2000). Similarly, 'mafic granites' of the Yilgarn Craton lie along, or near to, major structures (e.g. Cassidy et al., 1998). Hence, it can be speculated that the occurrence of sanukitoids in the Hercules Gneiss identifies the location of a pre-Albany–Fraser Orogen crustal-scale suture that originally separated two Archean terranes. Interestingly, an Archean granite from the Salmon Gums Au-prospect, nearly 600 km to the southwest of the Neale Project area, in the Munglinup Gneiss within the Northern Foreland of the Albany–Fraser Orogen, also falls within the sanukitoid field and may similarly suggest the presence of an old suture in that region as well. The location of this occurrence could be inferred as equivalent to the boundary between the

Youanmi Terrane and the Eastern Goldfields Superterrrane, now reworked within the Albany–Fraser Orogen. This rock yields a U–Pb zircon crystallization age of 2718 ± 11 Ma (Kirkland et al., 2013).

Granulite-facies zircons of the Hercules Gneiss

Gneissic samples from the Hercules Gneiss in the Tropicana Zone have complex U–Pb zircon age spectra reflecting both polyphase zircon growth and alteration processes. In this section, we further explore the possible zircon growth mechanisms. Such interpretation problems are not unique to these samples and have been discussed extensively with reference to the zircon geochronology of other high-grade Archean terranes and granulite-facies zircons elsewhere (Schaltegger et al., 1999; Whitehouse et al., 1997; 1999).

Granulite-facies zircon U–Pb systematics and internal textures

In the case of continuous U–Pb age distributions, two different approaches are typically applied. Analyses may be interpreted with the aid of CL images and ages defined based on textural similarities. However, in some cases, there is no unambiguous means to distinguish analyses, and indeed, several growth or alteration processes may have occurred simultaneously. Nonetheless, assuming that the observed data reflect zircon formed during a single magmatic event, the oldest concordant age could reflect the timing of that event. An alternative approach commonly used in the analysis of SIMS data from polyphase zircons again assumes that a single magmatic protolith age component is present and that the zircons have undergone younger Pb loss, resulting in a spread of ages. Successive rejection of the youngest ages from the weighted average is performed until the calculated MSWD reaches a threshold value at which assigned analytical errors alone are considered to account for the observed scatter of data. However, such a method is not based on independent petrographic information and may not yield a meaningful value for prolonged growth processes.

Sample GSWA 192531 yielded a range of concordant zircon ages from c. 2683 to 2585 Ma. All but three analyses are within two-sigma analytical uncertainty of concordia, and only one analysis is classified as having an intermediate degree of metamictization, based on calculations discussed in Murikami et al., (1991). Hence, the dataset demonstrably reflects crystalline zircons with concordant U–Pb systematics. There is a weak correlation between $^{207}Pb^*/^{206}Pb^*$ and common-Pb content (and in the dataset more generally), which may relate to slight over-correction for common Pb at low count rates around the level of background. Nonetheless, if common Pb correction is only applied when ^{204}Pb counts are above background, this trend disappears. In any case, the degree of common Pb correction is trivial and does not result in significant changes to calculated dates.

An alternative interpretation of the youngest 18 analyses in Group M could be that they reflect a magmatic, rather than metamorphic, genesis and the remaining analyses could therefore reflect the influence of inheritance. However, the zircon CL textures, which include concentric zoning, sector zoning, and homogeneous response, are characteristic of zircons regrown and altered under high-temperature conditions (Moller et al., 2002; Flowers et al., 2010). Alternatively, Group M could represent radiogenic-Pb loss from magmatic zircons. However, the analyses are within analytical uncertainty of concordia, the zircons are crystalline, and there is no correlation between uranium content and $^{207}Pb^*/^{206}Pb^*$ age, nor more derived measures including alpha dose and calculated density, arguing against a radiogenic Pb-loss interpretation (Fig. 12).

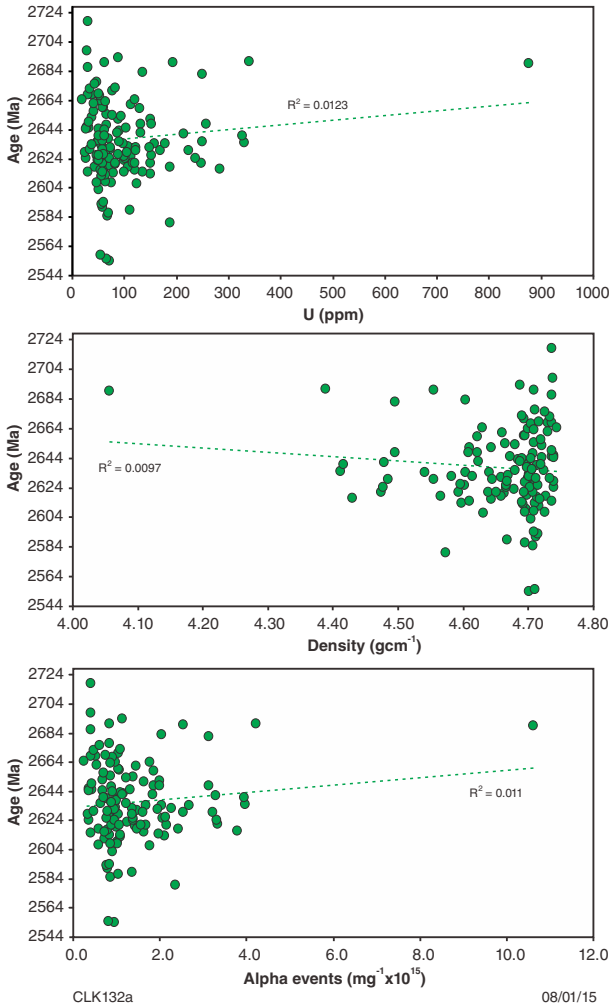

Figure 12. Group M age versus zircon uranium content (top), calculated apparent density (middle), and calculated apparent alpha events (lower). The lack of correlation between these measures and age provides no evidence for radiogenic-Pb loss being the dominant process leading to the dispersion of Group M dates on concordia.

Sample GSWA 192552 displays a very similar U–Pb pattern on a concordia diagram as GSWA 192531. All but two analyses are within two-sigma analytical uncertainty of concordia. Only six of 31 analyses are classified as intermediate and one as highly metamict with regard to alpha dose (Murikami et al., 1991). The youngest 13 analyses in Group M, yielding a $^{207}Pb^*/^{206}Pb^*$ date of 2641 ± 8 Ma, could be interpreted as magmatic, rather than metamorphic, and the remaining analyses could therefore be inherited. However, as with GSWA 192531, the zircon shapes and internal textures of Group M zircons are characteristic of crystals grown under granulite-facies conditions (Fig. 8). Alternatively, Group M could represent radiogenic-Pb loss from a single magmatic component (e.g. Pb loss from magmatic zircons). However, the vast majority of Group M analyses are within analytical uncertainty of concordia, Group M zircons are predominantly crystalline, and there is no correlation between uranium content and $^{207}Pb^*/^{206}Pb^*$ age. Furthermore, the fact that both cores (Group P) and rims (Group M) within both samples yield similar ages and that these ages span several million years, implies a prolonged process where at least some zircon growth was promoted by dissolution of cores, liberating zirconium to form new metamorphic overgrowths. The oldest date for zircon rims is 2698 ± 26 Ma (1σ), which is not significantly different from the date of 2726 ± 14 Ma for crystallization of zircon cores. This suggests that the rock was subjected to granulite-facies conditions in the lower crust very soon after crystallization of the protolith. The dispersion of dates in both protolith (Groups I and P) and granulite-facies zircons (Group M) is consistent with loss or redistribution of radiogenic Pb at high temperatures, as well as neocrystallization of zircon (Flowers et al., 2010).

Interpretation of zircon as 'metamorphic' poses significant challenges due to the numerous different mechanisms that can produce such zircon crystals, including subsolidus reactions that liberate zirconium (e.g. Fraser et al., 1997), crystallization from partial melts during high-grade metamorphism (anatectic melts, e.g. Schaltegger et al., 1999), or by dissolution–reprecipitation of pre-existing zircon with metamorphic fluids (e.g. Hoskin and Black, 2000). More than one of these crystallization mechanisms may operate in the same rock at essentially the same time (Kirkland et al., 2009) and it is highly likely that many of these so-called metamorphic growth mechanisms relate to processes in the presence of an aqueous or silicate fluid as opposed to the solid state (Corfu, 2003). Assuming radiogenic-Pb loss as the cause of U–Pb dispersion would suggest temperatures in excess of 1000°C (i.e. UHT conditions) that are sufficient to permit Pb diffusion in the crystalline zircon cores (Cherniak and Watson 2001). Alternatively, a zircon dissolution–reprecipitation process is also feasible to explain the dispersion of ages on a concordia diagram. In this situation, zircon cores would undergo dissolution to liberate prerequisite elements for new metamorphic zircon growth. Metamorphic zircon overgrowths would shield vestigial cores (e.g. minor undigested components) from further chemical interaction with fluid pathways (e.g. Ault et al., 2012). Such a process could be consistent with the observation that rims tend to be younger than cores within the same crystals. If dissolution was not stalled by new zircon growth, then it is feasible that core–rim age reversals could be observed.

Of relevance to the preceding discussion is our preferred interpretation of Group M zircons in sample GSWA 192530 from drillcore NLD080. Group M in this sample is interpreted to reflect granulite-facies zircon growth which peaked at the weighted mean $^{207}Pb^*/^{206}Pb^*$ date of 2623 ± 7 Ma (MSWD = 1.7). These analyses were located on zircons with CL textures characteristic of granulite-facies growth (Corfu, 2003). In contrast, oscillatory zoned zircons making up Group I are interpreted as magmatic cores which yield a much older concordia age of 2795 ± 12 Ma (MSWD = 0.66). Furthermore, CL images from this sample suggest that Group M zircons developed under conditions more closely approximating equilibrium in that they are essentially internally featureless and spherical, consistent with granulite-facies metamorphic zircon growth. Based on the similarity of the geochemical signature of this sample to the other granulite-facies meta-igneous rocks in the Hercules Gneiss, and the general rarity of sanukitoid magmatic events within the Yilgarn Craton and in other Archean cratons, the c. 2795 Ma age for these cores is anomalous. Hence, these zircon cores may represent a dominant inherited zircon component and reflect the magmatic crystallization of that source.

Timing of granulite-facies zircon growth in the Tropicana Zone

A total of 126 analyses of granulite-facies zircons (Group M), from seven samples of the Hercules Gneiss, yield $^{207}Pb^*/^{206}Pb^*$ dates of 2718–2554 Ma, which indicate a weighted average with an MSWD of >4, clearly implying geological sources of dispersion within the dataset (for this number of analyses, to have 95% confidence that the dispersion of dates can be accounted for by analytical precision alone, the MSWD value should approach unity), likely reflecting prolonged granulite-facies conditions (Fig. 13). The median $^{207}Pb^*/^{206}Pb^*$ date of 2634 ± 6 Ma for all Group M zircons may reflect the peak of granulite-facies zircon growth in the Tropicana Zone. In granulite-facies zircons (Group M) no correlation is evident between age and U, Th, alpha dose, or density, consistent with the dates reflecting prolonged growth rather than radiogenic-Pb loss or mobility.

Magmatic ages in relation to known components of the Yilgarn Craton

The drillcore samples from the Neale Project area have yielded a range of magmatic ages for protolith components in the Hercules Gneiss (or minimum age constraints on that protolith), as summarized in Table 1. Neoarchean magmatic activity, either indicated by inherited zircons or related to magmatic genesis directly in the sample, is indicated between 2826 and 2644 Ma. The oldest date for zircon rims in two samples (GSWA 192523 and GSWA 192552) is not significantly different from the date for

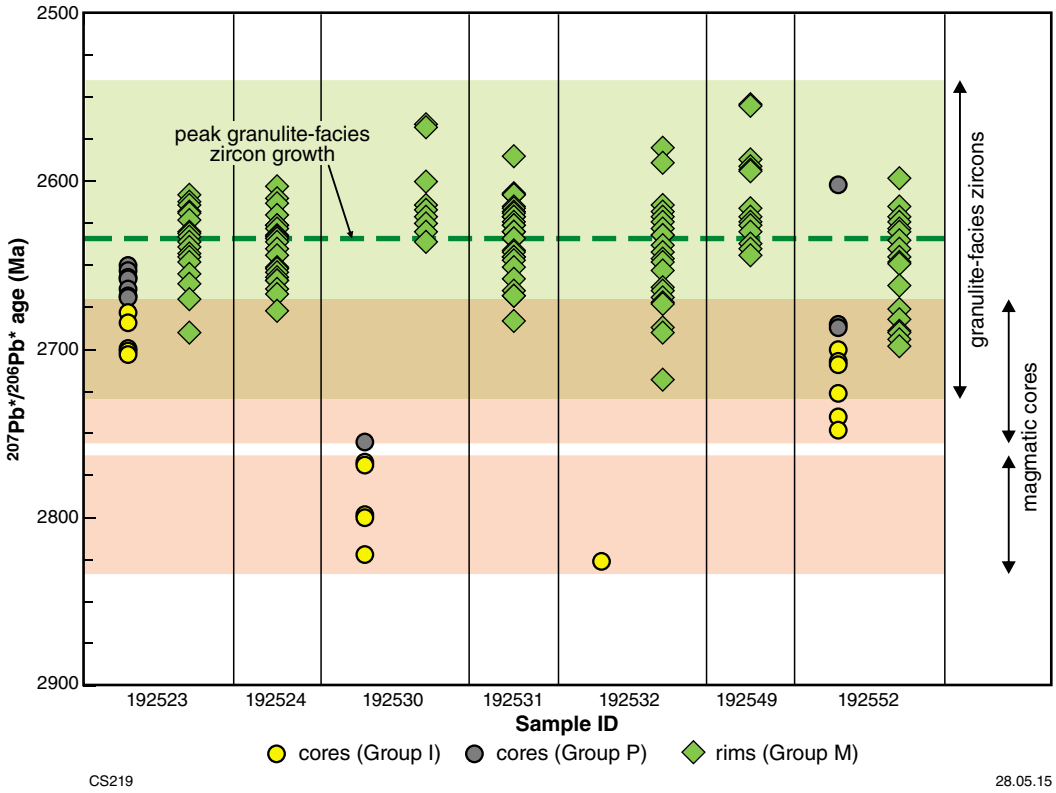

Figure 13. Dates for zircon cores and rims in Hercules Gneiss samples, illustrating the prolonged granulite-facies zircon growth event. The best age estimate for the sanukitoid protolith is estimated to be 2692 ± 16 Ma, based on GSWA 192523. Modified from Kirkland et al., (2015).

crystallization of oscillatory zoned zircon cores, which are interpreted to reflect magmatic crystallization in that specific rock. All of the samples (excluding the late microgranite vein GSWA 192550) indicate a consistent and prolonged granulite-facies zircon growth event. Furthermore, the similarity in age between rare vestigial cores and newly grown rims suggests that many, if not all, of these samples crystallized from a magmatic state shortly before or essentially coeval with granulite-facies conditions in the lower crust at c. 2700 Ma. Late-stage granite veins dated at 1783 ± 3 Ma cut the gneissic fabric in the granitic gneiss, which must have a magmatic crystallization age of at least c. 2644 Ma. Other evidence of late Paleoproterozoic events come from a metamorphic zircon rim in sample GSWA 192523, dated at c. 1770 Ma. These younger dates correspond with the Ngadju Event, during which dacitic rocks of the Voodoo Child Formation and the McKay Creek Metasyenogranite were emplaced (Less, 2013; Spaggiari et al., 2014b).

The magmatic rock record in the Yilgarn Craton extends back to at least c. 3080 Ma in the Youanmi Terrane in the west (Wang et al., 1998; Yeats et al., 1996; Van Kranendonk et al., 2013) and c. 2960 Ma in the Burtville Terrane in the northeast (Pawley et al., 2012) (Fig. 14). However, greenstone successions across the Yilgarn Craton are dominated by rocks that formed after c. 2820 Ma (Wyche et al., 2012). Because the Neale Project area lies to the east of the Yilgarn Craton, it is feasible that the Archean rocks of the Tropicana Zone were originally derived, either through rifting or transform processes, from this craton margin. However, the ages of magmatism and prolonged high-grade metamorphism have no unique correlatives in the easternmost components of the Yilgarn Craton, that is, the Eastern Goldfields Superterrane.

Pawley et al. (2012) discussed the timing of magmatism within the Eastern Goldfields Superterrane, and noted that the youngest granitic magmatism occurred at 2715–2630 Ma and involved several chemically distinct stages. West of the Eastern Goldfields Superterrane, within the Youanmi Terrane, lies the Southern Cross Domain, a broadly north–south region bounded by the Ida Fault to the east and the Youanmi and Kawana Faults to the west. Its southern boundary is truncated at about 45° by the Albany–Fraser Orogen. The major greenstone belts within this domain are the Ravensthorpe, Lake Johnston, Forrestania, Southern Cross, Marda, and Sandstone belts. Geochronology of the Southern Cross greenstones suggests that the successions range in age from <3130 Ma to 2732 Ma, with overlying clastic sedimentary rocks that are c. 2690 Ma old (Wang et al., 1996; Wyche et al., 2004). Geochemistry and geochronology of the granites and granitic gneisses of the Southern Cross Domain indicate emplacement commencing at 2815 Ma, with major

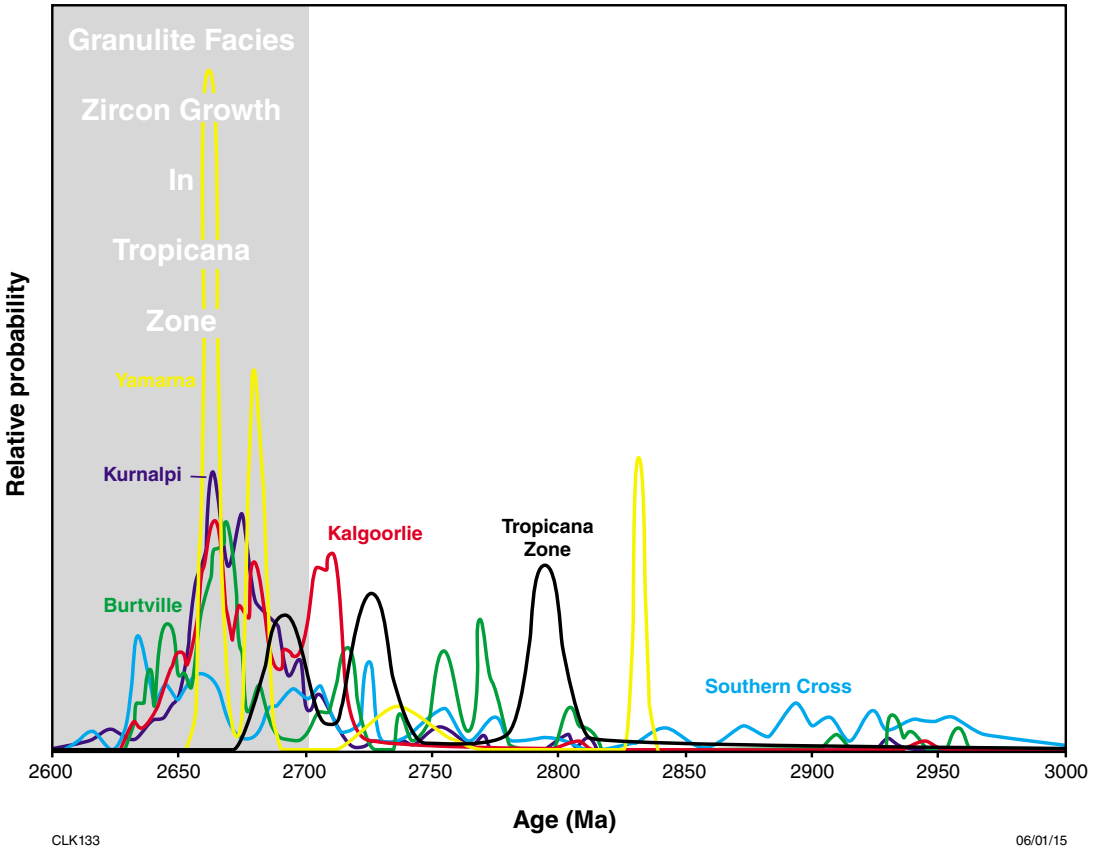

Figure 14. Relative probability diagram of magmatic zircon ages in various terranes and domains of the Yilgarn Craton in comparison to the ages of zircons in the Tropicana Zone

magmatic groups at 2735–2700 Ma, 2700–2670 Ma (high-Ca), and 2660–2600 Ma (low-Ca) (Archibald and Bettenay, 1977; Archibald et al., 1978), with a peak of granite activity occurring at c. 2700 Ma (Mole et al., 2012).

A statistical comparison between magmatic ages in protolith components of the Tropicana Zone with those in the Eastern Goldfields Superterrane and the Southern Cross Domain was performed using a Kolmogorov–Smirnov (K–S) test (Press et al., 1992) (Fig. 15). The K–S test is a nonparametric method for comparing cumulative probability distributions (Press et al., 1992). The test returns a P-value indicating the probability that random chance alone might produce the observed difference in two distributions drawn from the same parent population. A low probability indicates that differences between the two distributions are significant. We take a P-value of >0.05 to indicate that the differences between magmatic populations are not statistically significant and therefore that such regions have a similar magmatic heritage (Massey, 1951). This statistical evaluation indicates that the magmatic event history of the Tropicana Zone, based on the currently available magmatic crystallization age database, is indistinguishable at a >95% level to all of the various Yilgarn lithotectonic elements (Table 3). This result reflects the small sample set of protolith crystallization ages, and the prolonged reworking during granulite-facies metamorphism. Nonetheless, it does indicate that the magmatic histories of the Burtville Terrane and Southern Cross Domain appear to be the most similar to that in the Neale Project area.

The K–S test results indicate that the Burtville Terrane has the most similar magmatic age structure to that of the Tropicana Zone (Table 3). Evidence of c. 2800 Ma magmatism, including mafic magmatism, is widespread in the Yilgarn Craton, and has been interpreted to represent a period of rift-related tectonism and the cause of the north-northwest trending structural grain of the eastern Yilgarn Craton (Ivanic et al., 2012). The Hercules Gneiss yields inherited material (likely entrained on the sanukitoid emplacement pathway) with a magmatic crystallization age of 2795 ± 12 Ma (GSWA 192530), similar to magmatic crystallization ages in the Murchison and Southern Cross Domains of the Youanmi Terrane (e.g. GSWA 191056, Wingate et al., 2010; GSWA 178102, Wingate et al., 2008).

Initiation of granulite-facies metamorphism appears to have been essentially coeval with c. 2700 Ma magmatic crystallization in sanukitoids of the Tropicana Zone. Estimates of the original magmatic crystallization age of these rocks are hindered by the intense neocrystallization and reworking of zircon during granulite-facies metamorphism. Nonetheless, all rocks may have had a magmatic crystallization at c. 2700 Ma shortly preceding

granulite-facies zircon growth. Based on the unique geochemistry of these rocks, the age of this event could best be derived from the youngest oscillatory zoned zircon cores, which have textural characteristics that indicate growth within a viscous silicate melt and which have not been affected by radiogenic-Pb loss. Following this criteria, the date of 2692 ± 16 Ma for Group I zircons in sample GSWA 192523 is the best estimate for the timing of sanukitoid magmatism. Most other sanukitoid rocks in the Eastern Goldfields Superterrane were emplaced after the cessation of volcanism and high-Ca magmatism at c. 2655 Ma, which is later than the event in the Tropicana Zone. Given that pre-metamorphic vestigial cores are rare in the Hercules Gneiss, age-based correlations with many terranes and domains of Yilgarn Craton are feasible and an exotic origin unnecessary. Furthermore, the Archean granite from the Salmon Gums gold prospect has a sanukitoid composition and its U–Pb crystallization age of 2718 ± 11 Ma is similar to that inferred for the protolith of the Hercules Gneiss (Kirkland et al., 2013).

Implications of sanukitoid magmatism

The emergence of sanukitoid magmatism in the Archean likely signified the emergence of plate tectonic processes on Earth (Smithies et al., 2003, 2007; Pease et al., 2008) and compositionally similar magmas continue to be produced today — exclusively at subduction zones. Halla (2011) discussed the timing of sanukitoids in the Archean rock record, commencing at around 2950 Ma in the Pilbara Craton (Smithies and Champion, 2000) and 2870 Ma in the Amazonian Craton (de Oliveira et al., 2009), followed by progressive formation until the end of the Archean (western Yilgarn at 2760 Ma; eastern Karelia at 2740 Ma; western Karelia at 2720 Ma [Halla, 2005]; northern Superior at 2700 Ma, southern Superior at 2680 Ma, and eastern Yilgarn at 2.65 Ga). The latest Archean sanukitoids were formed between 2.6 and 2.5 Ga in the Kaapvaal and North China Cratons,

Table 3. Kolmogorov–Smirnov (KS) P-values and D-values, including the error in the cumulative density function for terranes and domains of the Yilgarn Craton compared to the Tropicana Zone

	Yamarna	*Burtville*	*Kurnalpi*	*Kalgoorlie*	*Hercules Gneiss*	*Youanmi*
Yamarna		0.166	0.211	0.152	0.359	0.365
Burtville	0.995		0.307	0.289	0.212	0.296
Kurnalpi	0.932	0.001		0.127	0.441	0.494
Kalgoorlie	0.998	0.001	0.249		0.432	0.447
Hercules Gneiss	0.759	0.937	0.155	0.164		0.252
Youanmi	0.380	0.009	0.000	0.000	0.825	

NOTE: Numbers in the matrix refer to the probability that any two geological units are sourced from the same age population, with consideration of the uncertainty in age measurement. The higher the P-value (shown in lower left of matrix), the more likely it is that the two age distributions being compared were drawn from the same population. P-values >0.05 (highlighted) imply a correlation at >95% confidence. P-values <0.05 indicate that the samples are from distinctly different populations. The upper half of the matrix shows D-values calculated from the distance between cumulative probability curves accounting for the uncertainty within the density function; critical values can be found in Massey (1951).

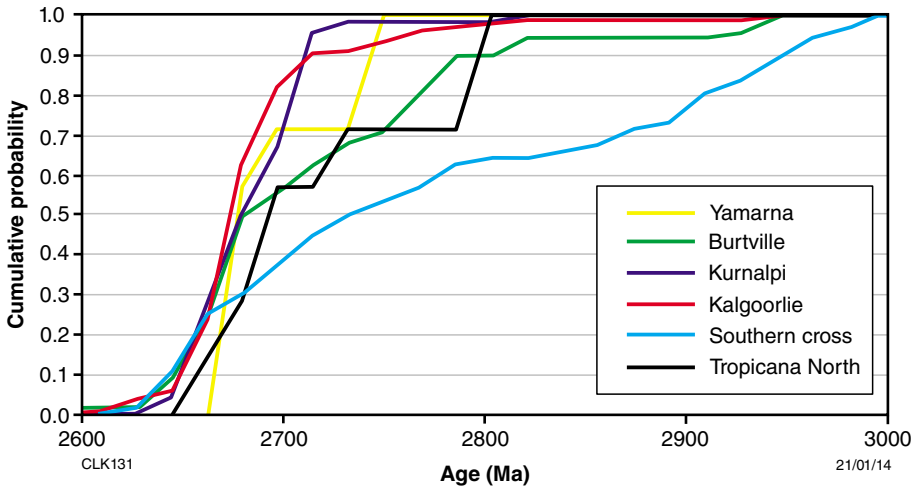

Figure 15. Cumulative probability plot of magmatic zircon ages for terranes and domains of the Yilgarn Craton in comparison to those in the Tropicana Zone (Neale Project area). The maximum horizontal distance between lines is a measure of the similarity of the age populations.

although Phanerozoic sanukitoids are also known from the Caledonian Orogen (Fowler and Rollinson, 2012). Typically, within each craton, the period(s) of sanukitoid magmatism is limited, occurring within a few tens of Ma after the cessation of TTG magmatism (Smithies and Champion, 2000).

Enrichment of the subcontinental lithospheric mantle with incompatible elements implies crustal recycling into the mantle and, in the case of sanukitoids from the Pilbara Craton, their association with other diagnostic magmas such as boninites, adakites, and high-Nb basalts, provides the earliest clear lithogeochemical evidence that plate tectonic processes had begun on Earth (Smithies and Champion, 2000; Smithies et al., 2003, 2005, 2007; Pease et al., 2008; Martin et al., 2005; 2009). Sanukitoids are derived through remelting of a mantle wedge, metasomatized earlier through introduction of adakitic melts derived by partial melting of a subducted slab (e.g. Stern et al., 1989; Evans and Hanson, 1997; Smithies and Champion, 2000; Martin et al., 2005). Apart from explaining many of the geochemical attributes of sanukitoids, and the compositional distinctions between these and true adakites (Martin et al., 2005), the suggestion that they are remelts of modified mantle explains why, in Archean settings, the intrusion of sanukitoids typically closely post-dates TTG magmatism (e.g. Stern et al., 1989; Evans and Hanson, 1997; Smithies and Champion, 2000). One suggested process for triggering sanukitoid magmatism is slab breakoff following attempted subduction of buoyant continental lithosphere during collisional processes (e.g. Van Kranendonk et al., 2007), although there is no a priori reason why other processes (e.g. slab tear) cannot also provide the required thermal impetus for remelting — and indeed, modern sanukitoids like those from the Aleutian Islands are unlikely to relate to slab breakoff processes. At least for Archean sanukitoids, the slab breakoff hypothesis is supported by numerical modelling (van Hunen and Moyen, 2012). Regardless of the trigger for melting, the suggestion that sanukitoid magmatism is diagnostic of convergent margin processes means that the occurrence of these rocks likely identifies mantle-tapping structures directly related to ancient plate boundaries.

Tropicana Zone metamorphism in comparison to Yilgarn Craton metamorphic history

The Yilgarn Craton has a complex metamorphic history, although the following broad processes have been suggested: (i) an early, low-pressure granulite-facies metamorphism, with high geothermal gradient, contemporaneous with the eruption of komatiites at 2715–2705 Ma (Wyche et al., 2012); (ii) later medium-pressure metamorphism likely due to exhumation of deep-seated early structures around granite domes (Goscombe et al., 2009; Wyche et al., 2012); (iii) subsequent periods of low-pressure metamorphism, accompanied by moderate to high geothermal gradients, reflect exhumation during granite doming prior to and during late-basin development; and (iv) very low pressures and geothermal gradients mark the end of granite doming and the initiation of exhumation (Goscombe et al., 2009). Such a thermal history appears distinctly different from the prolonged granulite-facies conditions, ranging from 2718–2554 Ma, implied for the Tropicana Zone, which may reflect a much lower crustal level than normally exposed within the Yilgarn Craton.

The mineralized samples in the Neale Project area were subjected to a low-grade chlorite–actinolite–'sericite' alteration. Biotite and clinozoisite–epidote may also occur as alteration phases, overprinting earlier igneous textures. Mesomylonite fabrics (e.g. in NLD046 at 129.9 – 130.1 m and in NLD080 at 60.7 – 60.85 m) indicate earlier metamorphic conditions >500 °C, although the minerals currently observed reflect the very latest stage of lower-grade alteration processes. Amphibole compositions corresponding to (ferro)gedrite have been identified by energy dispersive spectroscopy (EDS) in NLD071 (81.2 – 81.4 m) and NLD80 (83.88 – 84.05 m), and had an early paragenesis consistent with higher grades of metamorphism. Furthermore, the presence of gedrite, typically replaced by chlorite, indicates metamorphic grade of at least lower amphibolite facies. Gedrite itself appears as a replacement phase possibly growing after pyroxene, supporting earlier higher-grade conditions. Elsewhere in the Tropicana Zone, amphibolite-facies conditions, with localized granulite-facies conditions, have been indicated (Spaggiari et al., 2011; Doyle et al., 2015). Zircon CL textures, localized migmatitic zones, and the U–Pb isotopic dispersion along concordia are consistent with early granulite-facies conditions in the Hercules Gneiss.

Occurrences of other granulite-facies rocks in the Yilgarn Craton are limited. Czarnota et al. (2010) discussed a metamorphic event associated with high heat flow related to magmatic arc generation that produced granulites in the craton. Two granulite localities were discussed: one from the western Kurnalpi Terrane (Gindalbie Domain); and one from the western Burtville Terrane (Duketon Domain). In both cases, the rocks were mafic with orthopyroxene–clinopyroxene–hornblende–plagioclase assemblages. Pressure–temperature estimates from these rocks of 4.0 kbar and 740°C imply a geotherm of 56°C/km. Age constraints on and details of this Eastern Goldfields granulite–facies event are very sparse, but Czarnota et al. (2010) associated it with their Ma event at 2720–2685 Ma. The initiation of granulite-facies zircon growth in the Tropicana Zone is similar to, but dramatically outlasted, this Ma event.

The Narryer Terrane on the northwestern margin of the Yilgarn Craton represents another component of the Yilgarn Craton that has a granulite-facies history. The Narryer Terrane is dominated by quartzofeldspathic gneisses derived from 3.7 – 3.4 Ga granitic intrusions (e.g. Kinny et al., 1988), interlayered with minor deformed and metamorphosed banded iron-formation, mafic and ultramafic intrusive rocks, and metasedimentary rocks (Kinny et al., 1990). In the Narryer Terrane, granulite-facies metamorphism occurred at c. 3.3 Ga ago, at estimated conditions of 750–850°C and 7–10 kbar (Muhling, 1990). Components remained in the lower crust

for c. 1700 Ma following peak metamorphism and were exhumed only during a much younger tectonic event. In the Tropicana Zone, Doyle et al. (2015) suggested that a rutile U–Pb age of c. 2520 Ma records cooling through 500–550°C, with a biotite Ar–Ar cooling age of 2515 Ma reflecting exhumation along a retrograde path from peak granulite-facies conditions. Prolonged 2718–2554 Ma granulite-facies zircon growth in the Hercules Gneiss implies that the Tropicana Zone was held at a deep-crustal level before exhumation into greenschist-facies conditions by c. 2515 Ma. This exhumation was coeval with fluid migration along the Plumridge Detachment and an early phase of gold mineralization at c. 2520 Ma (Doyle et al., 2015).

Ages in relation to known components of the Albany–Fraser Orogen

The crystallization age of 1783 ± 3 Ma for a microgranite vein (GSWA 192550) intruded into an Archean granitic gneiss, which underwent granulite-facies zircon growth at 2616 ± 13 Ma (GSWA 192549), indicates Proterozoic overprinting of the Neale Project area rocks. Similarly, a single metamorphic zircon overgrowth at c. 1770 Ma from an amphibolitic gneiss (GSWA 192523), indicates Proterozoic overprinting of Archean rocks. Proterozoic zircon crystallization ages that are similar to these are widespread throughout the Albany–Fraser Orogen, and are part of the Ngadju Event (Spaggiari et al., 2014b,c). This event is represented in the Tropicana Zone by dacitic volcanic and ultramafic rocks of the Voodoo Child Formation (Less, 2013), and the McKay Creek Metasyenogranite, both of which occur just south of the Neale Project area. The presence of 1780–1770 Ma intrusions and overprinting indicates that the Hercules Gneiss was present during the Ngadju Event, and therefore was attached to the Yilgarn Craton by the late Paleoproterozoic as (para)autochthonous rocks in the same fashion as the Voodoo Child Formation and the McKay Creek Metasyenogranite, and the remainder of the Albany–Fraser Orogen (Spaggiari et al., 2011; Kirkland et al., 2011a).

Age of gold formation

In both Canada and Western Australia, there are many documented examples of lode-gold mineralization and associated wall-rock alteration that occurred late in the tectonic cycle, post-dating volcanism, sedimentation, some metamorphism, magmatic emplacement events, and deformation (e.g. Colvine et al., 1984; Wyche et al., 2012). In most lode gold instances in Western Australia, only minor deformation and limited intrusive activity post-dates mineralization and alteration (Yeats and Groves, 1998). Alteration, involving large volumes of hydrothermal fluid, is nearly invariably associated in time with the mineralizing event (Kendrick et al., 2011). Structurally induced permeability provides the main access for externally derived hydrothermal fluids (Vearncombe, 1998).

Pyrite grains in the Hercules Gneiss of the Tropicana Zone have had complex growth histories, as the rocks developed under a range of different structural and physical conditions during uplift and cooling of magmatic rocks. Gold growth accompanied several stages of pyrite development (Fig. 16) and hydrothermal alteration as evidenced by the mineral assemblage (biotite and muscovite, with varying amounts of actinolite, clinozoisite–epidote, and chlorite) associated with the gold and pyrite. Gold within drillcore NLD210 is developed as both very fine (≤25 μm) inclusions within pyrite as well as a fracture fill within pyrite. The highest grade gold (4.8 ppm Au) is associated with sulfides hosted in chloritic dilational structures in quartz veins. The quartz vein clearly post-dates metamorphic fabric development and is interpreted as part of a late brittle fracture set hosted within a mylonitic shear zone.

Pyrite within quartz vein material in NLD210 yields a Re–Os age of c. 2100 Ma, which is interpreted as the age of one generation of gold mineralization. More conservatively, this date must be a maximum age for generation of the gold infill within fractures in pyrite. Gold inclusions within pyrite indicate another older phase of gold mineralization in these rocks.

The Eastern Goldfields Superterrane contains more than 20 gold deposits with >1 million ounces of contained gold (Wyche et al., 2012). Within the superterrane, the Norseman–Wiluna greenstone belt contains significant lode-gold deposits. These gold deposits are confined to the volcanic–intrusive–sedimentary sequences of the greenstone belts rather than the granitic rocks. Much of the mineralization took place between 2650 and 2630 Ma, associated with strike-slip reactivation of earlier faults (normal and reverse), and was broadly synchronous with peak metamorphic conditions (Vielreicher et al., 2010). An earlier gold forming event at 2660–2655 Ma was associated with major extension (normal faulting and granite doming) and resulted in the formation of late basins and the intrusion of mantle-derived magmas and tight anticlockwise *PTt* paths (Said et al., 2011).

At least some of the gold mineralization within the Tropicana Zone at c. 2100 Ma is considerably later than that in the Eastern Goldfields terranes. Specifically, sulfides and gold have a late paragenesis in the Hercules Gneiss samples and are most commonly associated with biotite and muscovite, and with varying amounts of actinolite, clinozoisite–epidote, and chlorite. Other Proterozoic gold mineralization events are known from the northern edge of the Yilgarn Craton in the Marymia Inlier at c. 2200, 1830, and 1730–1660 Ma (Gazley et al., 2011), which hosts the estimated 10.5 million ounce Plutonic mine (McMillan, 1996; Vickery, 2004,).

Archean sanukitoids are known to be a fertile gold source at depth (Lin and Beakhouse, 2013). A spatial association between sanukitoids and gold mineralization has been noted elsewhere (e.g. Smithies and Champion, 1999; Kudryashov et al., 2013), and this extends to the Yilgarn Craton where several major gold deposits and prospects, including Lawlers, Kanowna Belle, Granny Smith, Liberty, Golden Cities, and Porphyry, are directly related

to sanukitoids (e.g. Champion and Sheraton, 1997). The observation that the Archean granites of the Neale Project area are sanukitoids might be particularly important not only in terms of the tectonic history of the region, but also the economic prospectivity — including a plausible explanation for the significant gold endowment of this part of the Albany–Fraser Orogen at the Tropicana–Havana deposit. The Tropicana Zone sanukitoids are perhaps most compositionally similar to the sanukitoids at the Mount Percy gold mine, near Kalgoorlie.

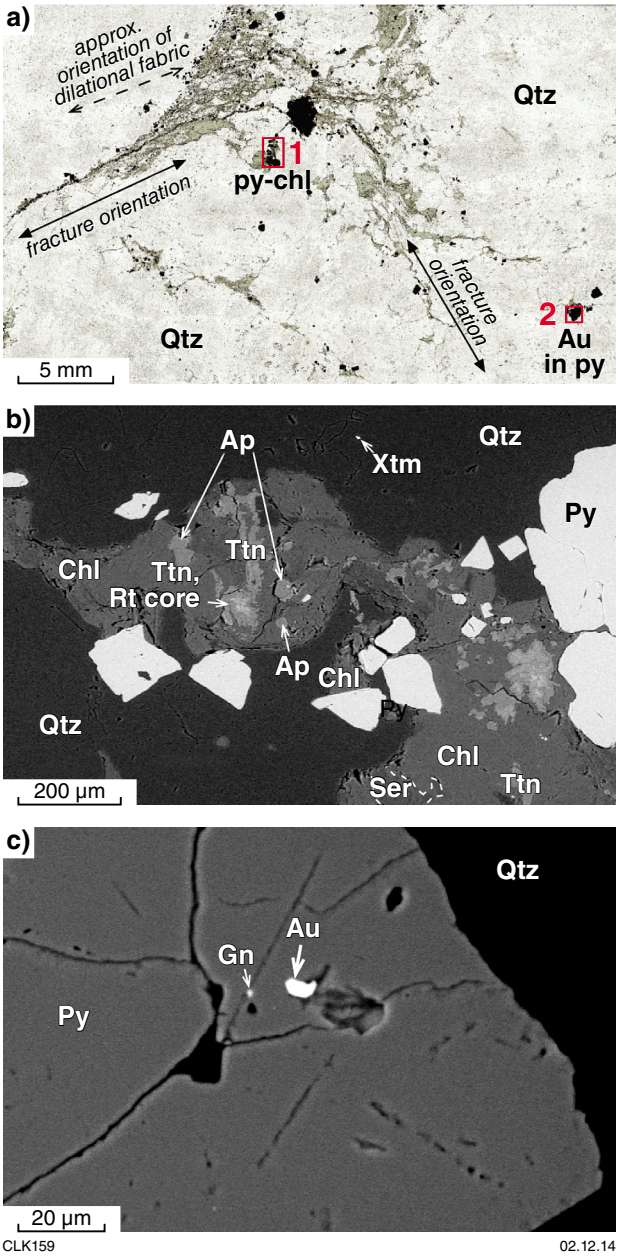

Figure 16. a) Transmitted-light image of chlorite–pyrite segregations and fracture fillings, and their structural relationships; b) BSE image of chloritic (Chl) infill at (1), displaying association with pyrite (Py), and inclusions of titanite (Ttn), rutile (Rt) and apatite (Ap). Xtm denotes xenotime hosted in quartz (Qtz). Ser denotes sericite replacing chlorite; c) Back-scattered electron (BSE) image of gold grain with proximal galena (Gn), in pyrite (Py) at (2)

The specific process of mineralization in the Tropicana Zone remains unknown, but it was likely associated with early Proterozoic fluid mobility and fabric development that extracted and concentrated metals from an Archean sanukitoid source. This metal-bearing fluid was channelled into brittle fractures which crystallized gold and biotite–pyrite–quartz at c. 2100 Ma. Texturally older disseminated pyrite with gold inclusions probably reflects an earlier phase of mineralization that occurred at or after 2500 Ma (Doyle et al., 2013, 2015).

Conclusions

At 2826–2644 Ma, the age of magmatic protolith components in the Hercules Gneiss of the Tropicana Zone is similar to those of many intrusive events within the Yilgarn Craton. However, the best age estimate of sanukitoid magmatism at 2692 ± 16 Ma is dissimilar to the ages of most other sanukitoids elsewhere within the Yilgarn Craton, although a sanukitoid 600 km to the southwest in the Albany–Fraser Orogen, on the extrapolated boundary between the Youanmi Terrane and the Eastern Goldfields Superterrrane, yields a similar age to the Tropicana Zone sanukitoids. Furthermore, although granulite-facies metamorphic zircon growth at 2718–2554 Ma was prolonged compared to the durations of similar events in the Yilgarn Craton, the timing of its initiation may match those of some granulite-facies events in the Eastern Goldfields Superterrane.

This may indicate that the Archean rocks of the Tropicana Zone reflect a deeper crustal level, or a different part of the Yilgarn Craton, or both, and suggest that the Tropicana Zone is a piece of the Yilgarn Craton not exposed elsewhere, now thrust northwest onto the Yamarna Terrane. The presence of Paleoproterozoic granites intruded into both the Hercules Gneiss during the 1780–1760 Ma Ngadju Event, which affected much of the Albany–Fraser Orogen, indicates that the Tropicana Zone was located close to its present position at or before this time. The timing of gold mineralization in the Neale Project area, at c. 2100 Ma, was most likely coeval with pyrite growth during late alteration processes and brittle fracturing, and significantly post-dates peak metamorphic conditions. This mineralization event does not obviously correlate with major Proterozoic tectono-thermal events known elsewhere in the Albany–Fraser Orogen. Gold was moved before the major Proterozoic magmatic and metamorphic events, including the Biranup Orogeny and Stages I and II of the Albany–Fraser Orogeny. The granitic gneisses of the Neale Project area and the Hercules Gneiss in the Tropicana Zone represent a single suite of sanukitoid magmatic rocks. As sanukitoid intrusions are well known for gold fertility we suggest that this is the primary source of gold in the Neale Project area, and that gold was subsequently remobilized and concentrated into brittle structures associated with pyrite, quartz, biotite, muscovite, actinolite, clinozoisite–epidote, and chlorite. The tracking of such magma types along crustal-scale structures on craton margins offers an important tool to vector towards Au mineralized domains.

References

Archibald, NJ and Bettenay, LF 1977, Indirect evidence for tectonic reactivation of a pre-greenstone sialic basement in Western Australia: Earth and Planetary Science Letters v. 33, p. 370–378.

Archibald, NJ, Bettenay, LF, Binns, RA, Groves, DI and Gunthorpe, RJ 1978, The evolution of Archaean greenstone terrains, Eastern Goldfields Province, Western Australia: Precambrian Research v. 6, p. 103–131.

Ault, AK, Flowers, RM and Mahan, KH 2012, Quartz shielding of sub-10 μm zircons from radiation damage-enhanced Pb loss: an example from a metamorphosed mafic dike, northwestern Wyoming craton: Earth and Planetary Science Letters, v. 339–340, p. 57–66.

Beeson, J, Harris, LB and Delour, CP 1995, Structure of the western Albany Mobile Belt (southwestern Australia): evidence for overprinting by Neoproterozoic shear zones of the Darling Mobile Belt: Precambrian Research, v. 75, p. 47–63, doi:10.1016/0301-9268(95)00017-Y.

Blenkinsop, TG and Doyle, MG 2014, Structural controls on gold mineralisation on the margin of the Yilgarn Craton, Albany–Fraser Orogen: The Tropicana deposit, Western Australia: Journal of Structural Geology, v. 67 p. 189–204.

Brisbout, LI, Spaggiari, CV and Aitken, ARA 2014, Integrating outcrop, aeromagnetic and gravity data: models of the east Albany–Fraser Orogen, *in* Albany–Fraser Orogen seismic and magnetotelluric (MT) workshop 2014: extended abstracts *compiled by* CV Spaggiari and IM Tyler: Geological Survey of Western Australia, Record 2014/6, p. 102–117.

Cassidy, KF, Champion, DC, Krapež, B, Barley, ME, Brown, SJA, Blewett, RS, Groenewald, PB and Tyler, IM 2006, A revised geological framework for the Yilgarn Craton, Western Australia: Geological Survey of Western Australia, Record 2006/8, 8p.

Cassidy, KF, Groves, DI and McNaughton, NJ, 1998, Late-Archean granitoid hosted lode-gold deposits, Yilgarn Craton, Western Australia: deposit characteristics, crustal architecture and implications for ore genesis: Ore Geology Reviews, v. 13, p. 65–102.

Champion, DC and Sheraton, JW 1997, Geochemistry and Nd isotope systematics of Archaean granites of the Eastern Goldfields, Yilgarn Craton, Australia: implications for crustal growth processes: Precambrian Research, v. 83, p. 109–132.

Champion, DC and Smithies, RH 2007, Geochemistry of Paleoarchean granites of the East Pilbara Terrane, Pilbara Craton, Western Australia: implications for early Archean crustal growth, *in* Earth's Oldest Rocks *edited by* MJ Van Kranendonk, RH Smithies, and V Bennett: Developments in Precambrian Geology, Elsevier, Amsterdam, v. 15, p. 369–410.

Cherniak, DJ, and Watson, EB 2001, Pb diffusion in zircon: Chemical Geology, v. 172, no. 1, p. 5–24.

Chesley, JT and Ruiz, J 1998, Crust–mantle interaction in large igneous provinces: implications from the Re–Os isotope systematics of the Columbia River flood basalts, Earth and Planetary Science Letters, v. 154, p. 1–11.

Clark, C, Kirkland, CL, Spaggiari, CV, Oorschot, C, Wingate, MTD and Taylor, R 2014, Proterozoic granulite formation driven by mafic magmatism: an example from the Fraser Range Metamorphics, Western Australia, v. 240, p. 1–21.

Clark, DJ, Hensen, BJ and Kinny, PD 2000, Geochronological constraints for a two-stage history of the Albany–Fraser Orogen, Western Australia: Precambrian Research, v. 102, no. 3, p. 155–183.

Clark, DJ, Kinny, PD, Post, NJ and Hensen, BJ 1999, Relationships between magmatism, metamorphism and deformation in the Fraser Complex, Western Australia: constraints from new SHRIMP U–Pb zircon geochronology: Australian Journal of Earth Sciences, v. 46, p. 923–932.

Colvine, AC, Andrews, AJ, Cherry, ME, Durocher, ME, Fyon, AJ, Lavigne Jr, MJ, Macdonald, MJ, Marmont, S, Poulsen, KH, Springer, JS and Troop, DG 1984, An integrated model for the origin of Archean lode gold deposits: Ontario Geological Survey, Open file report 5524, 98p.

Coney, PJ, Jones, DL and Monger, JWH 1980, Cordilleran suspect terranes: Nature, v. 288, p. 329–333.

Corfu, F 2003, Atlas of zircon textures: Reviews in Mineralogy and Geochemistry, v. 53, no. 1, p. 469–500.

Czarnota, K, Champion, DC, Cassidy, KF, Goscombe, B, Blewett, RS, Henson, PA, and Groenewald, PB 2010, Geodynamics of the Eastern Goldfields Superterrane: Precambrian Research, v. 183, p. 175–202.

Dawson, GC, Krapež, B, Fletcher, IR, McNaughton, N and Rasmussen, B 2003, 1.2 Ga thermal metamorphism in the Albany–Fraser Orogen of Western Australia: consequence of collision or regional heating by dyke swarms?: Journal of the Geological Society, London, v. 160, p. 29–37.

de Oliveira, MA, Dall'Agnol, R, Althoff, FJ and da Silva Leite, AA 2009, Mesoarchean sanukitoid rocks of the Rio Maria Granite-Greenstone Terrane, Amazonian Craton, Brazil: Journal of South American Earth Sciences, v. 27, no. 2, p. 146–160.

Doyle, M, Gibbs, D, Savage, J and Blenkinsop, T 2009, Geology of the Tropicana Gold Project, Western Australia, *in* Smart Science for Exploration and Mining: Economic Geology Research Unit, James Cook University; Proceedings of the 10th Biennial SGA Meeting of the Society for Geology Applied to Mineral Deposits, Townsville, Queensland, 17 August, v. 1, p. 50–52.

Doyle, M, Kendall, B, Gibbs, D and Kent, M 2008, Tropicana deposit: a new gold province in Western Australia. Geological Society of Australia, in New generation advances in geoscience: Geological Society of Australia; Australian Earth Sciences Convention (AESC) 2008, Perth, Western Australia, 21 July, Abstracts 89, p. 85.

Doyle, M, Savage, J, Blenkinsop, TG, Crawford, A and McNaughton, N 2013, Tropicana – unravelling the complexity of a +6 million ounce gold deposit hosted in granulite facies metamorphic rocks: World Gold Conference Brisbane, The Australasian Institute of Mining and Metallurgy, Publication series no. 9/2013, p. 87–93.

Doyle, M, Blenkinsop, T, Crawford, A, Fletcher, I, Foster, J, Fox-Wallace, LJ, Large, R, Mathur R, McNaughton, N, Meffre, S, Muhling, J, Occhipinti, S, Rasmussen, B and Savage, J 2014, Tropicana deposit, Western Australia: an integrated approach to understanding granulite-hosted gold and the Tropicana Gneiss, *in* Albany-Fraser Orogen seismic and magnetotelluric (MT) workshop 2014: extended abstracts *compiled by* CV Spaggiari and IM Tyler: Geological Survey of Western Australia, Record 2014/6, p. 69–76.

Doyle, MG, Fletcher, IR, Foster, J, Large, R, Mathur, R, McNaughton, NJ, Meffre, S, Muhling, JR, Phillips, D and Rasmussen, B 2015, Geochronological constraints on the Tropicana gold deposit and Albany–Fraser Orogen, Western Australia: Economic Geology, in press.

Evans, OC and Hanson, GN 1997, Late-to post-kinematic Archean granitoids of the SW Superior Province: derivation through direct mantle melting, in Greenstone Belts edited by MJ de Wit, and LD Ashwal: Oxford University Press, p. 280–295.

Fowler, M, and Rollinson, H 2012, Phanerozoic sanukitoids from Caledonian Scotland: Implications for Archean subduction: Geology, v. 40, no. 12, p. 1079–1082.

Flowers, RM, Schmitt, AK and Grove, M 2010, Decoupling of U–Pb dates from chemical and crystallographic domains in granulite facies zircon: Chemical Geology, v. 270, no. 1, p. 20–30.

Fraser, G, Ellis, D and Eggins, S 1997, Zirconium abundance in granulite-facies minerals, with implications for zircon geochronology in high-grade rocks: Geology, v. 25, no. 7, p. 607.

Fox-Wallace, LJ 2010, Geology of the Hat Trick Prospect in the Tropicana Project area, Western Australia: James Cook University, Australia, BSc. (Honours) thesis (unpublished), 104p.

Gazley, MF, Vry, JK and Boorman, JC 2011, P–T evolution in greenstone-belt mafic amphibolites: an example from Plutonic Gold Mine, Marymia Inlier, Western Australia: Journal of Metamorphic Geology, v. 29, p. 685–698.

Gazley, MF, Vry, JK, du Plessis, E and Handler, MR 2011, Application of portable X-ray fluorescence analyses to metabasalt stratigraphy, Plutonic Gold Mine, Western Australia: Journal of Geochemical Exploration, v. 110, no. 2, p. 74–80.

Goddard, O 2010, EIS Final Report, Tropicana East (Neale E38/1913): Geological Survey of Western Australia, Statutory mineral exploration report, A093703 (unpublished).

Goldfarb, RJ, Groves, DI and Gardoll, S 2001, Orogenic gold and geological time: a global synthesis: Ore Geology Reviews, v. 18, p. 1–75.

Goscombe, B, Blewett, RS, Czarnota, K, Groenewald, PB and Maas, R 2009, Metamorphic evolution and integrated terrane analysis of the eastern Yilgarn Craton: rationale, methods, outcomes and interpretation: Geoscience Australia, Record 2009/23, 270p.

Groves, DI, Condie, KC, Goldfarb, RJ, Hronsky, JMA and Vielreicher, RM 2005, Secular changes in global tectonic processes and their influence on the temporal distribution of gold-bearing mineral deposits: Economic Geology, v. 100, p. 203–224.

Halla, J 2005, Late Archean high-Mg granitoids (sanukitoids) in the southern Karelian domain, eastern Finland: Pb and Nd isotopic constraints on crust−mantle interactions: Lithos, v. 79, no. 1, p. 161–178.

Halla, J 2011, Sanukitoid granitoids as indicators of accretionary tectonics from the late Mesoarchean to the Archean–Proterozoic boundary, EGU General Assembly 2011, Geophysical Research Abstracts, v. 13, EGU2011-7916, 2011.

Hoskin, PWO and Black, LP 2000, Metamorphic zircon formation by solid-state recrystallisation of protolith igneous zircon: Journal of Metamorphic Geology, v. 18, p. 423– 439.

Hronsky, JMA, Groves, DI, Loucks, RR and Begg, GC 2012, A unified model for gold mineralisation in accretionary orogens and implications for regional-scale exploration targeting methods: Mineralium Deposita, v. 47, no. 1.

Ivanic, TJ, Van Kranendonk, MJ, Kirkland, CL, Wyche, S, Wingate, MTD and Belousova, EA 2012, Zircon Lu–Hf isotopes and geochemistry of the Murchison Domain of the Yilgarn Craton: Eoarchean crust reworked during Meso-Neoarchean plume-driven magmatism: Lithos, v. 148, p. 112–127.

Kendrick, MA, Honda, M, Walshe, J and Petersen K 2011, Fluid sources and the role of abiogenic-CH 4 in Archean gold mineralization: constraints from noble gases and halogens: Precambrian Research, v. 189, no. 3, p. 313–327.

Kinny, PD, Williams, IS, Froude, DO, Ireland, TR and Compston, W 1988, Early Archaean zircon ages from orthogneisses and anorthosites at Mount Narryer, Western Australia: Precambrian Research, v. 38, p. 325–341.

Kinny, PD, Wijbrans, JR, Froude, DO, Williams, IS and Compston, W 1990, Age constraints on the geological evolution of the Narryer Gneiss Complex, Western Australia: Australian Journal of Earth Science, v. 37, p. 51–69.

Kirkland, CL, Spaggiari, CV, Pawley, MJ, Wingate, MTD, Smithies, RH, Howard, HM, Tyler, IM, Belousova, EA and Poujol, M 2011a, On the edge: U–Pb, Lu–Hf, and Sm–Nd data suggests reworking of the Yilgarn Craton margin during formation of the Albany–Fraser Orogen: Precambrian Research, v. 187, p. 223–247, doi:10.1016/j.precamres.2011.03.002.

Kirkland, CL, Whitehouse, M and Slagstad, T 2009, Fluid-assisted zircon and monazite growth within a shear zone: a case study from Finnmark, Arctic Norway: Contributions to Mineralogy and Petrology, v. 158, no. 5, p. 637–657.

Kirkland, CL, Spaggiari, CV, Wingate, MTD, Smithies, RH, Belousova, EA, Murphy, R and Pawley, MJ 2011b, Inferences on crust–mantle interaction from Lu–Hf isotopes: a case study from the Albany–Fraser Orogen: Geological Survey of Western Australia, Record 2011/12, 25p.

Kirkland, CL, Wingate, MTD, Spaggiari, CV and Pawley, MJ 2010, 194737: metasyenogranite, Bobbie Point; Geochronology Record 866: Geological Survey of Western Australia, 4p.

Kirkland, CL, Wingate, MTD and Spaggiari, CV 2012, 194784: metamonzogranite, Newman Rock; Geochronology Record 1026: Geological Survey of Western Australia, 4p.

Kirkland, CL, Wingate, MTD and Spaggiari, CV 2013, 192507: granitic gneiss, Bishops Road; Geochronology Record 1088: Geological Survey of Western Australia, 4p.

Kirkland, CL, Spaggiari, CV, Smithies, RH, Wingate, MTD, Belousova, EA, Gréau, Y, Sweetapple, MT, Watkins, R, Tessalina, S, and Creaser, R 2015, The affinity of Archean crust on the Yilgarn—Albany–Fraser Orogen boundary: Implications for gold mineralization in the Tropicana Zone: Precambrian Research, in press.

Kudryashov, NM, Petrovsky, MN, Mokrushin, AV and Elizarov, DV 2013, Neoarchean sanukitoid magmatism in the Kola region: geological, petrochemical, geochronological, and isotopic-geochemical data: Petrology, v. 21, p. 351–374.

Less, T 2013, Newly recognised Paleoproterzoic gold–silver mineralisation in the Albany–Fraser Orogeny, *in* Future understanding of tectonics, ores, resources, environment and sustainability *edited by* Z Chang, R Goldfarb, T Blenkinsop, C Palczek, D Cooke, K Camuti and J Carranza: FUTORES Conference, Economic Geology Research Unit Contribution 68, James Cook University, Townsville, Australia 2–5 June, p. 31.

Lin, S and Beakhouse, GP 2013, Synchronous vertical and horizontal tectonism at late stages of Archean cratonization and genesis of Hemlo gold deposit, Superior Craton, Ontario, Canada: Geology, v. 41, no. 3, p. 359.

Ludwig, KR 1998, On the treatment of concordant uranium–lead ages: Geochimica et Cosmochimica Acta, v. 62, p. 665–676.

Ludwig, KR 2003, User's manual for Isoplot 3.00: a geochronological toolkit for Microsoft Excel: Berkeley Geochronology Center, Special Publication 4, 74p.

Ludwig, KR 2009, Squid 2.50, a user's manual: Berkeley Geochronology Center, Berkeley, California, USA (unpublished report), 95p.

Massey, FJ 1951, The Kolmogorov–Smirnov test for goodness of fit: Journal of the American Statistical Association, v. 46, p. 68–78.

Markey, R, Stein, HJ, Hannah, JL, Selby, D and Creaser, RA 2007, Standardizing Re-Os geochronology: a new molybdenite reference material (Henderson, USA) and the stoichiometry of Os salts: Chemical Geology, v. 244, p. 74–87.

Markey, RJ, Stein, HJ and Morgan, JW 1998, Highly precise Re–Os dating for molybdenite using alkaline fusion and NTIMS: Talanta, v. 45, p. 935–946.

Martin, H, Moyen, J-F and Rapp, R 2009, The sanukitoid series: magmatism at the Archaean–Proterozoic transition: Earth and Environmental Science Transactions of the Royal Society of Edinburgh, v. 100, p. 15–33.

Martin, H, Smithies, RH, Rapp, R, Moyen, J-F and Champion, D 2005, An overview of adakite, tonalite–trondhjemite–granodiorite (TTG), and sanukitoid: relationships and some implications for crustal evolution: Lithos, v. 79, p. 1–24.

McMillan, NM 1996, Late-Archaean, syn-amphibolite facies, lode-gold deposits overprinted by Palaeoproterozoic deformation, metasomatism and hydrothermal activity at Marymia, Western Australia: University of Western Australia, PhD thesis (unpublished).

Mole, DR, Fiorentini, ML, Thebaud, N, McCuaig, TC, Cassidy, KF, Kirkland, CL, Wingate, MTD, Romano, SS, Doublier, MP and Belousova, EA 2012, Spatio-temporal constraints on lithospheric development in the southwest–central Yilgarn Craton, Western Australia: An International Geoscience Journal of the Geological Society of Australia, v. 59, no. 5, p. 625–656.

Moller, A, O'Brien, P, Kennedy, A and Kroner A 2002, Polyphase zircon in ultrahigh-temperature granulites (Rogaland, SW Norway): constraints for Pb diffusion in zircon: Journal of Metamorphic Geology, v. 20, p. 727–740.

Morelli, RM, Creaser, RA, Selby, D, Kontak, DJ and Horne, RJ 2005, Rhenium–osmium arsenopyrite geochronology of Meguma Group gold deposits, Meguma terrane, Nova Scotia, Canada: evidence for multiple mineralizing events: Economic Geology and the Bulletin of the Society of Economic Geologists, v. 100, p. 1229–1242.

Morris, PA 2000, Composition of Geological Survey of Western Australia geochemical reference materials: Geological Survey of Western Australia, Record 2000/11, 33p.

Morris, PA 2007, Composition of the Bunbury Basalt (BB1) and kerba Monzogranite (KG1) geochemical reference materials, and assessing the contamination effects of mill heads: Geological Survey of Western Australia, Record 2007/14, 22p.

Murikami, T, Chakoumakos, BC, Ewing, RC, Lumpkin, GR and Weber, WJ 1991, Alpha-decay event damage in zircon: American Mineralogist, v. 76, p. 1510–1532.

Muhling, JR 1990, The Narryer Gneiss Complex of the Yilgarn Block, Western Australia: a segment of Archaean lower crust uplifted during Proterozoic orogeny: Journal of Metamorphic Geology, v. 8, p. 47–64.

Myers, JS 1990, Albany–Fraser Orogen, in Geology and mineral resources of Western Australia: Geological Survey of Western Australia, Memoir 3, p. 255–263.

Nelson, DR, Myers, JS and Nutman, AP 1995, Chronology and evolution of the Middle Proterozoic Albany–Fraser Orogen, Western Australia: Australian Journal of Earth Sciences, v. 42, p. 481–495.

Nesbitt, HW and Young, GM 1982, Early Proterozoic climates and plate motions inferred from major element chemistry of lutites: Nature, v. 299, p. 715–717.

Occhipinti, SA, Doyle, M, Spaggiari CV, Korsch, R, Cant, G, Martin, K, Kirkland, CL, Savage, J, Less, T, Bergin, L and Foz, L 2014, Preliminary interpretation of the deep seismic reflection line 12GA–T1: northeastern Albany–Fraser Orogen, *in* Albany–Fraser Orogen seismic and magnetotelluric (MT) workshop 2014: extended abstracts *compiled by* CV Spaggiari and IM Tyler: Geological Survey of Western Australia, Record 2014/6, p. 52–68.

Oorschot, CW 2011, P–T–t evolution of the Fraser Zone, Albany–Fraser Orogen, Western Australia: Geological Survey of Western Australia, Record 2011/18, 101p.

Pawley, MJ, Wingate, MTD, Kirkland, CL, Wyche, S, Hall, CE, Romano, SS and Doublier, MP 2012, Adding pieces to the puzzle: episodic crustal growth and a new terrane in the northeast Yilgarn Craton, Western Australia: Australian Journal of Earth Sciences, v. 59, p. 603–623.

Pease, V, Percival, J, Smithies, H, Stevens, G and Van Kranendonk, M 2008, When did plate tectonics begin? Evidence from the orogenic record, *in* When did plate tectonics begin on planet Earth? *edited by* KC Condie and V Pease: Geological Society of America, Special paper 440, p. 199–228.

Press, WH, Flannery, BP, Teukolsky, SA and Vetterling, WT 1992, Numerical recipes in C: the art of scientific computing: Cambridge University Press, ISBN 0-521-43108-5.

Roberts, MP and Finger, F 1997, Do U–Pb zircon ages from granulites reflect peak metamorphic conditions?: Geology v. 25, p. 319– 322.

Said, N, Kerrich, R, Maier, WD and McCuaig, C 2011, Behaviour of Ni–PGE–Au–Cu in mafic–ultramafic volcanic suites of the 2.7 Ga Kambalda Sequence, Kalgoorlie Terrane, Yilgarn Craton: Geochimica et Cosmochimica Acta, v. 75, no. 10, p. 2882–2910.

Saunders, EJ 2006, Pressure–temperature–composition–time constraints of the Tropicana gold deposit, Western Australia: University of Western Australia, BSc. (Honours) thesis (unpublished), 98p.

Schaltegger, U, Fanning, CM, Günther, D, Maurin, JC, Schulmann, K and Gebauer, D 1999, Growth, annealing and recrystallisation of zircon and preservation of monazite in high-grade metamorphism: conventional and in-situ U–Pb isotope, cathodoluminescence and microchemical evidence: Contributions to Mineralogy and Petrology v. 134, p. 186–201.

Selby, D and Creaser, RA 2004, Macroscale NTIMS and mircoscale LA-MC-ICP-MS Re–Os isotopic analysis of molybdenite: testing spatial restriction for reliable Re–Os age determinations, and implications for the decoupling of Re and Os within molybdenite: Geochimica et Cosmochimica Acta, v. 68, no. 19, p. 3897–3908.

Shirey, SB and Hanson, GN 1984, Mantle-derived Archaean monzodiorites and trachyandesites: Nature, v. 310, p. 222–224.

Sirius 2013, 15 July Australian Securitires Exchange announcement, Maiden Bollinger Resource Estimate and Scoping Study Update.

Sillitoe, RH 2008, Major gold deposits and belts of the North and South American Cordillera: distribution, tectonomagmatic settings and metallogenic considerations: Economic Geology, v. 103, p. 663–688.

Solomon, M 1990, Subduction, arc reversal and the origin of porphyry copper–gold deposits in island arcs: Geology, v. 18, p. 630–633.

Smithies, RH, Howard, HM, Evins, PM, Kirkland, CL, Kelsey, DE, Hand, M, Wingate, MTD, Collins, AS and Belousova, E 2011, High-temperature granite magmatism, crust–mantle interaction and the Mesoproterozoic intracontinental evolution of the Musgrave Province, Central Australia: Journal of Petrology, v. 52, no. 5, p. 931–958.

Smithies, RH and Champion, DC 1999, High-Mg diorite from the Archaean Pilbara Craton; anorogenic magmas derived from a subduction-modified mantle: Geological Survey of Western Australia, Annual Review, 1998–99, p. 45–49.

Smithies, RH and Champion, DC 2000, The Archaean high-Mg diorite suite: links to tonalite–trondhjemite–granodiorite magmatism and implications for Early Archaean crustal growth: Journal of Petrology, v. 41, p. 1653–1671.

Smithies, RH, Champion, DC and Cassidy, KF 2003, Formation of Earth's Early Archaean continental crust: Precambrian Research, v. 127, p. 89–101.

Smithies, RH, Champion, DC, Van Kranendonk, MJ, Howard, HM and Hickman, AH 2005, Modern-style subduction processes in the Mesoarchaean: geochemical evidence from the 3.12 Ga Whundo intra-oceanic arc: Earth and Planetary Science Letters, v. 231, p. 221–237.

Smithies, RH, Spaggiari, CV, Kirkland, and Maier, WD 2014 Geochemistry and petrogenesis of igneous rocks in the Albany–Fraser Orogen, *in* Albany–Fraser Orogen seismic and magnetotelluric (MT) workshop 2014: extended abstracts *compiled by* CV Spaggiari and IM Tyler: Geological Survey of Western Australia, Record 2014/6, p. 77–88.

Smithies, RH, Van Kranendonk, MJ and Champion, DC 2007, The Mesoarchean emergence of modern style subduction: Gondwana Research, v. 11, p. 50–68.

Spaggiari, CV, Bodorkos, S, Barquero-Molina, M, Tyler, IM and Wingate, MTD 2009, Interpreted bedrock geology of the south Yilgarn and central Albany–Fraser Orogen, Western Australia: Geological Survey of Western Australia, Record 2009/10, 84p.

Spaggiari, CV, Kirkland, CL, Pawley, MJ, Smithies, RH, Wingate, MTD, Doyle, MG, Blenkinsop, TG, Clark, C, Oorschot, CW, Fox, LJ and Savage, J 2011, The geology of the east Albany–Fraser Orogen — a field guide: Geological Survey of Western Australia, Record 2011/23, 97p.

Spaggiari, CV and Occhipinti, SA 2014, Interpreted pre-Mesozoic bedrock geology of the northeast region of the Albany–Fraser Orogen including seismic line GA12–T1 (1:250 000), *in* Albany–Fraser Orogen seismic and magnetotelluric (MT) workshop 2014: extended abstracts *compiled by* CV Spaggiari and IM Tyler: Geological Survey of Western Australia, Record 2014/6, Plate 1.

Spaggiari, CV, Kirkland, CL, Smithies, RH, and Wingate, MTD, 2014a, Tectonic links between Proterozoic sedimentary cycles, basin formation and magmatism in the Albany–Fraser Orogen, Western Australia Geological Survey, Report 133, 63p.

Spaggiari, CV, Kirkland, CL, Smithies, RH, Occhipinti, SA and Wingate, MTD 2014b, Geological framework of the Albany–Fraser Orogen, *in* Albany–Fraser Orogen seismic and magnetotelluric (MT) workshop 2014: extended abstracts *compiled by* CV Spaggiari and IM Tyler: Geological Survey of Western Australia, Record 2014/6, p. 12–27.

Spaggiari, CV, Occhipinti, SA, Korsch, RJ, Doublier, MP, Clark, DJ, Dentith, MC, Gessner, K, Doyle, MG, Tyler, IM, Kennett, BLN, Costelloe, RD, Fomin, T and Holzschuh, J 2014c, Interpretation of Albany–Fraser seismic lines 12GA-AF1, 12GA-AF2 and 12GA-AF3: implications for crustal architecture, *in* Albany–Fraser Orogen seismic and magnetotelluric (MT) workshop 2014: extended abstracts *compiled by* CV Spaggiari and IM Tyler: Geological Survey of Western Australia, Record 2014/6 p. 28–51.

Stacey, JS and Kramers, JD 1975, Approximation of terrestrial lead isotope evolution by a two-stage model: Earth and Planetary Science Letters, v. 26, p. 207–221.

Steiger, RH and Jäger, E 1977, Subcommission on geochronology: convention on the use of decay constants in geo- and cosmochronology: Earth and Planetary Science Letters, v. 36, p. 359–362.

Stern, RA 2001, A new isotopic and trace-element standard for the ion microprobe: preliminary thermal ionization mass spectrometry (TIMS) U–Pb and electron-microprobe data: Geological Survey of Canada, Radiogenic Age and Isotopic Studies, Report 14, Current Research 2001–F1, 11p.

Stern, RA, Bodorkos, S, Kamo, SL, Hickman, AH and Corfu, F 2009, Measurement of SIMS instrumental mass fractionation of Pb isotopes during zircon dating: Geostandards and Geoanalytical Research, v. 33, p. 145–168.

Stern, RA, Hanson, GN and Shirey, SB 1989, Petrogenesis of mantle-derived, LILE-enriched Archean monzodiorites and trachyandesites (sanukitoids) in southwestern Superior Province: Canadian Journal of Earth Sciences, v. 26, p. 1688–1712.

Stokes, MA 2014, Structural evolution of the Pleiades Lakes Region; northeastern Albany–Fraser Orogen, Western Australia: Geological Survey of Western Australia, Record 2014/15, 145p.

Tichomirowa, M, Whitehouse, MJ and Nasdala, L 2005, Resorption, growth, solid state recrystallisation, and annealing of granulite facies zircon — a case study from the Central Erzgebirge, Bohemian Massif: Lithos, v. 82, no. 1, p. 25–50.

Tohver, E, Bettencourt, JS, Tosdal, R, Mezger, K, Leite, WB, Payolla, BL 2004, Terrane transfer during the Grenville orogeny: tracing the Amazonian ancestry of southern Appalachian basement through Pb and Nd isotopes, Earth and Planetary Science Letters, 2004, v. 228, p. 161–176.

Van Hunen, J and Moyen, J-F 2012, Archean subduction: fact or fiction?: Annual Review of Earth and Planetary Sciences, v. 40, no. 1, p. 195–219.

Van Kranendonk, MJ, Ivanic, TJ, Wingate, MTD, Kirkland, CL and Wyche, S 2013, Long-lived, autochthonous development of the Archean Murchison Domain, Yilgarn Craton: Precambrian Research, v. 229, p. 49–92.

Van Kranendonk, MJ, Smithies, RH, Hickman, HH and Champion, DC 2007, Review: secular tectonic evolution of Archean continental crust: interplay between horizontal and vertical processes in the formation of the Pilbara Craton, Australia: Terra Nova, v. 19, p. 1–38.

Vearncombe, JR 1998, Shear zones, fault networks, and Archean gold: Geology, v. 26, no. 9, p. 855.

Vickery, NM 2004, The Plutonic gold deposit, Western Australia: Geology and Geochemistry of an Archaean orogenic gold system, University of New England, Australia, PhD thesis (unpublished), 593p.

Vielreicher, NM, Groves, DI, Snee, LW, Fletcher, IR and McNaughton, NJ 2010, Broad synchroneity of three gold mineralization styles in the Kalgoorlie gold field: SHRIMP, U–Pb, and $^{40}Ar/^{39}Ar$ geochronological evidence: Economic Geology, v. 105, p. 187–227.

Wang, Q, Schiotte, L and Campbell, IH 1996, Geochronological constraints on the age of komatiites and nickel mineralisation in the Lake Johnston greenstone belt, Yilgarn Craton, Western Australia: Australian Journal of Earth Sciences v. 43, p. 381–385.

Wang, Q, Schiotte, L and Campbell, IH 1998, Geochronology of the supracrustal rocks from the Golden Grove area, Murchison Province, Yilgarn block, Western Australia: Australian Journal of Earth Sciences, v. 45, p. 571–577.

Watkins, R 2012, Australian Securites Exchange announcement 24/4/12 (ASX code BDR), Beadell Resources Limited, Tropicana East – Hercules Drill Results, 4p.

Whitehouse, MJ, Claesson, S, Sunde, T and Vestin, J 1997, Ionmicroprobe U–Pb zircon geochronology and correlation of Archaean gneisses from the Lewisian Complex of Gruinard Bay, north-west Scotland: Geochimica et Cosmochimica Acta, v. 61, p. 4429– 4438.

Whitehouse, MJ, Kamber, BS and Moorbath, S 1999, Age significance of U–Th–Pb zircon data from Early Archaean rocks of West Greenland—a reassessment based on combined ion-microprobe and imaging studies: Chemical Geology, v. 160, p. 201–224.

Wingate, MTD and Kirkland, CL 2013, Introduction to geochronology information released in 2009, Geological Survey of Western Australia, 5p.

Wingate, MTD, Bodorkos, S and Kirkland, CL 2008, 178102: hornblende tonalite, Finger Post Bore; Geochronology dataset 727 in Compilation of geochronology data: Geological Survey of Western Australia.

Wingate, MTD, Kirkland, CL and Ivanic, TJ 2010, 191056: gabbronorite, Kockalocka Bore; Geochronology Record 898: Geological Survey of Western Australia, 4p.

Wyche, S, Fiorentini, ML, Miller, JL and McCuaig, TC 2012, Geology and controls on mineralisation in the Eastern Goldfields region, Yilgarn Craton, Western Australia: Episodes, v. 35, p. 273–282.

Wyche, S, Nelson, DR and Riganti, A 2004, 4350–3130 Ma detrital zircons in the Southern Cross Granite–greenstone terrane, Western Australia: implications for the early evolution of the Yilgarn Craton: Australian Journal of Earth Sciences, v. 51, p. 31–45.

Yeats, CJ and Groves, DI 1998, The Archaean Mount Gibson gold deposits, Yilgarn Craton, Western Australia: products of combined synvolcanic and syntectonic alteration and mineralisation: Ore Geology Reviews, v. 13, no. 1, p. 103–129.

Yeats, CJ, McNaughton, NJ and Groves, DI 1996, SHRIMP U–Pb geochronological constraints on Archean volcanic-hosted massive sulfide and lode gold mineralization at Mount Gibson, Yilgarn Craton, Western Australia: Economic Geology, v. 91, p. 1354–1371.

RECORD 2015/5

TEMPORAL CONSTRAINTS ON MAGMATISM, GRANULITE-FACIES METAMORPHISM, AND GOLD MINERALIZATION OF THE HERCULES GNEISS, TROPICANA ZONE, ALBANY–FRASER OROGEN

Kirkland et al.

This Record is published in digital format (PDF) and is available as a free download from the DMP website at <www.dmp.wa.gov.au/GSWApublications>.

Further details of geological products produced by the Geological Survey of Western Australia can be obtained by contacting:

Information Centre
Department of Mines and Petroleum
100 Plain Street
EAST PERTH WESTERN AUSTRALIA 6004
Phone: +61 8 9222 3459 Fax: +61 8 9222 3444
www.dmp.wa.gov.au/GSWApublications